Lawrence Berkeley National Laboratory

Title

Developing Soil Gas and 222Rn Entry Potentials for Substructure Surfaces and Assessing Rn Control Diagnostic Techniques

Permalink

https://escholarship.org/uc/item/5q91v3sz

Authors

Turk, B H
Harrison, J
Prill, R J
et al.

Publication Date

1989-03-01

Copyright Information

Lawrence Berkeley Laboratory
UNIVERSITY OF CALIFORNIA

APPLIED SCIENCE DIVISION

Developing Soil Gas and ^{222}Rn Entry Potentials
for Substructure Surfaces and Assessing Rn Control
Diagnostic Techniques

B.H. Turk, J. Harrison, R.J. Prill, and R.G. Sextro

March 1989
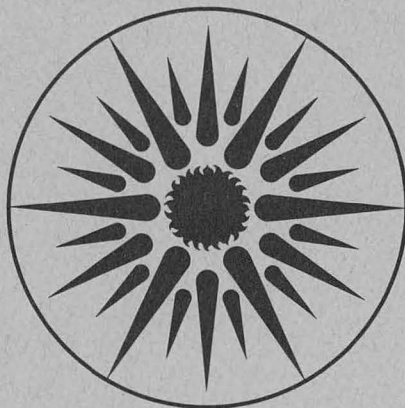
APPLIED SCIENCE DIVISION

DISCLAIMER

DEVELOPING SOIL GAS AND ^{222}Rn ENTRY POTENTIALS FOR SUBSTRUCTURE SURFACES AND ASSESSING Rn CONTROL DIAGNOSTIC TECHNIQUES

Bradley H. Turk, Jed Harrison,* Richard J. Prill,[+]
and Richard G. Sextro

Indoor Environment Program
Applied Science Division
Lawrence Berkeley Laboratory
1 Cyclotron Road
Berkeley, CA   94720

March 1989

*Current Address: Office of Radiation Programs, U.S. Environmental Protection Agency, 401 M Street SW, Washington, D.C. 20460

[+]Current Address: Washington State Energy Extension Service, N. 1212 Washington, Spokane, WA 99201

ABSTRACT

Research-based procedures for characterizing the causes of elevated indoor ^{222}Rn levels and guiding the selection of an appropriate control technique were evaluated at seven New Jersey houses. Procedures such as thorough visual inspections, blower door air leakage tests, pressure field mapping, subsurface vacuum extension tests, sampling of ^{222}Rn concentrations throughout the substructure, and measurements of the additional depressurization caused by various appliances all were found to furnish important information to the contractor or researcher. An analysis of data from these and other diagnostic techniques performed at the seven houses also indicates: (1) regions of very high permeability existed directly adjacent to the exterior of substructure walls and floors, (2) the additional substructure depressurization caused by operation of forced-air furnaces and attic exhaust fans could exceed 1 Pascal, (3) ^{222}Rn concentrations below basement slabs and slabs-on-grade adjoining below grade basement walls were approximately seven times higher than those within block wall cavities, and (4) air leakage areas of substructure ceilings were quite large, ranging up to 0.15 m^2. The pressure field mapping tests identified the areas surrounding the substructure that were well coupled to the indoors. Using flow, pressure difference, and ^{222}Rn concentration data, indices of soil gas entry potential and ^{222}Rn entry potential were developed to indicate the areas of the substructure that may have high entry rates of soil gas and ^{222}Rn, respectively. These indices could be helpful for quantifying the relative resistance to soil gas movement of substructure surfaces and surrounding soils, and for determining the placement of Rn control systems.

OVERVIEW

To develop an effective and efficient system for long-term control of elevated ^{222}Rn in a building requires a thorough understanding of the interaction of the building and its systems with the movement of ^{222}Rn in the soil. To assist researchers and private-commercial contractors, a number of procedures and measurement techniques (diagnostic techniques) have been developed to improve our knowledge of Rn entry and of practical Rn control methods

2

(Brennan 1988; Harrje et al. 1987; Gadsby et al. 1988; Sanchez et al. 1987). Radon-222 control diagnostic techniques are a set of tests and procedures that are systematically applied to a structure with high indoor ^{222}Rn levels for the purposes of: (1) identifying the source(s) of ^{222}Rn; (2) understanding the mechanisms by which ^{222}Rn interacts with and enters the building; and (3) selecting, designing, and installing an appropriate control technique that will effectively and economically reduce long-term ^{222}Rn levels below accepted guidelines under changing conditions of environment and occupancy.

This paper is the continuation of an exploratory study, begun in 1986, of the utility of various diagnostic techniques in seven New Jersey homes. The preliminary work has been previously reported in Turk et al. 1987a. An objective of this work was to develop and evaluate diagnostic techniques to assist in the design, installation, and operation of appropriate Rn control systems. Another practical goal was to reduce the winter indoor ^{222}Rn levels in these houses to below the U.S. Environmental Protection Agency (EPA) guideline for annual concentrations of 148 Bq m^{-3} (4 pCi l^{-1}). Because they are part of a research effort, some of the techniques described here may have broader application to the study of soil gas (and ^{222}Rn) transport. Others, in their present form, may be of limited practical use to contractors. This study was based on preliminary evaluations of diagnostic techniques conducted in 15 houses in the Pacific Northwest (Turk et al. 1987b).

DESCRIPTION OF PROCEDURES

The general sequence of events leading to the installation of a Rn control system in a house can be briefly described, as follows. Diagnostic procedures are initiated after elevated indoor ^{222}Rn levels have been confirmed. While the pressure-driven flow of soil gas (containing ^{222}Rn) into buildings is the primary cause of elevated indoor ^{222}Rn levels in the vast majority of structures, an inspection of the building can suggest whether possible non-soil sources (domestic water and building materials) should be tested. The structure and entry points are further characterized through various tests and measurements. An appropriate mitigation system or technique is then designed and installed, followed by short-term

3

measurements of indoor ^{222}Rn levels and system operating parameters. If necessary, the system is modified to improve its effectiveness, again verified by short-term measurements, and long-term follow-up monitoring of indoor ^{222}Rn levels begins.

While other mitigation techniques may be necessary in certain situations, subsurface ventilation (SSV) through depressurization (SSD) or pressurization (SSP) is successful in most houses. Consequently, many of the diagnostic tests are directed towards the design and implementation of this type of system. Brief descriptions of the prospective diagnostic techniques are provided in the following paragraphs. More complete descriptions of these diagnostic techniques, the criteria used for selection of the mitigation systems, and descriptions of the systems and their performance are provided in Turk et al. 1987a and Turk et al. 1988a.

(1) Visual Inspection

The visual inspection consisted of a complete tour of the building with the owner/occupant and building plans, if available. In addition, standarized forms (Turk et al. 1987a) were completed that requested pertinent information on construction characteristics, substructure holes and imperfections that open to the soil, mechanical system operation, and occupant effects (window openings, appliance operation, occupancy times and locations, etc.). A floor plan was sketched and dimensioned. Photographs were sometimes helpful, including any that were taken during construction of the substructure.

If the water supply was from a private well or the municipal supply was known to have elevated levels of ^{222}Rn, then it was noted that the water was a possible significant source of indoor ^{222}Rn. Likewise, it was also noted if the house had large quantities of exposed earth-based materials that might be suspected of containing significant radionuclide mineralization.

(2) Building Material Surface ^{222}Rn Flux

A metal pan (21.6 cm diameter), containing two charcoal adsorption canisters, was sealed with a non-drying putty or caulk to the surfaces of building materials suspected of having high ^{222}Rn emanation rates (walls, floors, etc.) caused by excess ^{226}Ra in the material. After exposure for 24 to 48 hours, the canisters were analyzed by gamma spectrometry and the ^{222}Rn flux from the surfaces was calculated. The uncertainty in the calculated ^{222}Rn flux is

4

estimated at ±20%. The contribution to indoor air [222]Rn concentrations was estimated from the [222]Rn flux normalized by indoor volume

$$F_v = (FA)/V,\qquad\qquad [1]$$

where F_v =   normalized flux (Bq/m^3-s),
         F   =   flux (Bq/m^2-s),
         A   =   material surface area (m^2), and
         V   =   building/zone volume (m^3).

If a ventilation rate of 0.5 air changes per hour (ach) is assumed for a building, then a value of F_v greater than 0.021 Bq/m^3-s may indicate that [222]Rn flux from the building materials could contribute more than 148 Bq m^{-3} to the indoor air.

(3) <u>Radon-222-in-Water</u>

Research suggests that [222]Rn concentrations in the domestic water supply will cause [222]Rn concentrations in indoor air that are approximately 10000 times lower (Gesell and Pritchard 1980; Nazaroff et al. 1985). In this study, two methods were used to determine the [222]Rn concentrations in the domestic water supplies. The direct method involved collecting samples of water in one liter polyethylene bottles from faucets where the water was not filtered or aerated. The [222]Rn activity in the bottles was then analyzed by gamma spectrometry. Samples were collected twice; in the late fall of 1986 and in August of 1987. The estimated uncertainty for collection and analysis is 10%. Concentrations of [222]Rn in water greater than 1.5×10^6 Bq m^{-3} indicated that the water may be a strong source of indoor [222]Rn.

An alternative technique was performed from two to four times at each house. A bathroom shower was operated for 10 to 15 minutes with the bathroom door closed and ventilation systems off. Grab samples of bathroom air were collected before and after the shower was operated. The [222]Rn concentrations (C(t) and C(o), respectively in Bq m^{-3}) along with the elapsed time, t (h); room volume, V (m^3); shower flow rate, W (m^{3}h^{-1}); and a transfer coefficient, E, of 0.9 were used to estimate concentrations of [222]Rn in water, C_w (Bq m^{-3}), from

$$C_w = [V(C(t) - C(o))]/EWt .\qquad\qquad [2]$$

(4) Appliance Effects

The operation of many devices often found in residences (exhaust fans, clothes dryers, combustion devices, and forced air furnaces) can cause additional depressurization of substructures (Mowris and Fisk 1987). These devices were cycled on and off up to 20 times while substructure-outside pressure differences were monitored. The change in the average pressure difference when the device is cycled between "on" and "off" is the additional depressurization (or pressurization) experienced by the substructure during appliance operation.

(5) Soil Air Permeability

A device that meters air at various pressures from a pressurized cylinder into a probe inserted into the soil was used to determine soil air permeability (DSMA Atcon Ltd. 1983). These measurements were made at approximately 25 locations in the soil outside each house at depths ranging from 0.3 m to 2.2 m and distances from the houses ranging from 0.5 m to 3.5 m. The data may help to identify regions of soil where soil gas (including Rn) is more readily transported to the substructure.

In each house, approximately 30 test holes (6 mm to 13 mm in diameter) were drilled through substructure slab floors and hollow block walls, and into the block cavities of these walls (approximately 0.25 m above the floor) for a variety of measurement purposes. Permeability was measured at a distance of 0.01 to 0.02 m from the exterior of the structure through several of the test holes. A few measurement locations extended approximately 1 m below the slab floors. These data describe the approximate permeability of near-house materials and may indicate the presence of gaps and channels between the building and these materials.

(6) Blower Door Tests

Depressurization by a blower door was used used to determine the effective leakage area (ELA) of each house and of the zones within each house (superstructure, substructure). The ELA for the whole house was measured with the door to the substructure open. The ELA for the superstructure was measured with the door closed, but with the substructure windows and

6

vents open. The substructure ELA was measured by placing the blower door at the door to the substructure, and with the superstructure doors and windows open. ELAs for the substructure ceiling and substructure walls and floor were then calculated from:

$$ELA_c = (ELA_p + ELA_b - ELA_w)/2, \text{ and} \qquad [3]$$

$$ELA_f = ELA_b - ELA_c, \qquad [4]$$

where:

ELA_w = whole building ELA,
ELA_p = superstructure ELA,
ELA_b = substructure ELA,
ELA_c = substructure ceiling ELA, and
ELA_f = substructure basement walls and floor ELA.

The flow-calibrated blower door was also used to pressurize basements to determine the flows necessary to achieve successful Rn control by basement overpressurization of a few Pascals. A power curve was fitted to the blower door data so that flows could be calculated at pressure differences other than those used in the test.

(7) Grab Samples of ^{222}Rn

To identify areas of high ^{222}Rn gas concentration, samples of air were collected from outdoor and indoor test holes, and suspected entry points using evacuated alpha-scintillation cells. Indoor samples were collected under both natural environmental conditions and during a 10 Pa depressurization of the substructure that was imposed by the blower door. Errors in ^{222}Rn concentrations measured with this procedure were approximately ± 20%.

(8) Subsurface Air Flow and Vacuum Field Extension

A single-speed industrial vacuum pulled air through a test hole in the slab floors and depressurized the subslab space to simulate a subsurface depressurization mitigation system. During vacuum operation, pressure differences (referenced to the basement with the test holes sealed) and air velocities (with the test holes open) were measured at the other test holes throughout the basement to determine the extent and spatial distribution of the pressure field. Those test holes with the largest pressure differences and flow rates were better connected to the vacuum hole (i.e., the resistance to flow between the vacuum and test holes is less); thus an

SSD system would be more likely to control soil gas and Rn entry near these test holes.

(9) Pressure Field Mapping

The substructure of each building was depressurized with a blower door to approximately −30 Pa, while pressure differences, referenced to the basement, were measured at the outdoor soil probe locations and at several of the indoor test holes (Nazaroff et al. 1986). Additional tests were conducted at approximately −30 Pa and −10 Pa in some of the houses. In these later tests, more of the indoor test hole locations were surveyed and air velocities at test holes were measured. Pressure differences across the test holes were measured with the test holes sealed and velocities with the test holes open. Ratios of the pressure differences at the test holes or soil probes to the basement depressurization relative to outside (coupling ratios) provide a measure of the extension of the pressure fields from the house. Smaller ratios may result from nearby cracks and openings in the substructure surfaces or from more distant openings that are connected via high permeability pathways to the test holes, and therefore indicate good coupling with the interior of the substructure. Air velocities as small as approximately 0.025 m s^{-1} were measured with a hot wire anemometer attached to a flow adaptor designed to mate with the test holes (Figure 1). At velocities of 0.7 m s^{-1}, the pressure drop across the flow adaptor was estimated to be approximately 0.5 Pa. Small quantities of chemical smoke were directed at the surface of the test holes to provide qualitative information on the relative velocity and direction of the air moving through the test holes.

DATA PRESENTATION

Examples of data are shown on a site plan for house LBL14C in Figures 2 and 3. Table 1 is a key for the symbols used in the drawings. Similar data for the remaining six houses and other data from diagnostic measurements in all houses are presented in Appendices A through C.

(1) Building Material Surface ^{222}Rn Flux

The emanation of ^{222}Rn from the surfaces of building materials varied by more than three orders of magnitude. A flux of 0.0009 Bq/m^2-s was measured at one floor (LBL09) and one

block wall (LBL14) location, 0.47 Bq/m²-s (LBL10) at one block wall location, and 1.9 Bq/m²-s (LBL10) on another block wall. The high fluxes measured on the block wall surfaces may be erroneous due to diffusion of ^{222}Rn from the block cavity through the block surface or to a poor seal between the measurement pan and the irregular surface of the block. For all houses tested, the mean flux from 10 measurements on concrete slab floors is 0.013 Bq/m²-s (geometric mean (GM) of 0.0085 Bq/m²-s, geometric standard deviation (GSD) of 3.2) and the mean flux from 13 measurements on block walls is 0.24 Bq/m²-s (GM of 0.033 Bq/m²-s, GSD of 9.9). If the one extremely high flux from a block wall surface is eliminated, the mean for walls becomes 0.10 Bq/m²-s (GM of 0.024 Bq/m²-s, GSD of 7.6). These data can be compared with the range of 0.0009 Bq/m²-s to 0.0067 Bq/m²-s for earth-based construction materials presented in Nero and Nazaroff 1984. Corresponding ^{222}Rn entry rates were calculated by multiplying the flux by the appropriate surface area (m²). The building volume-normalized source rate (F_v) was estimated for each house. Only the source rate of 0.074 Bq/m³-s at LBL10 using the suspect high flux data exceeded the target of 0.021 Bq/m³-s. There was no other information to suggest that the block walls in this house comprised radium-rich materials. The data from all houses are compiled in Table A1 in Appendix A.

(2) Radon-222-in-Water

Direct gamma spectrometric analysis of ^{222}Rn concentrations in water showed a range of 4100 Bq m^{-3} (at LBL13) to 310,000 Bq m^{-3} (at LBL08 with a private well). Differences between the two seasonal samples (collected at 6 houses) were quite large; ranging from 31,000 to 39,000 Bq m^{-3} at LBL12, 135,000 to 310,000 Bq m^{-3} at LBL08, and 8100 to 46,000 Bq m^{-3} at LBL10. None of these ^{222}Rn-in-water concentrations are expected to contribute more than approximately 30 Bq m^{-3} to the indoor air concentrations.

The alternate method of measuring bathroom air concentrations before and after shower operation yielded disappointing results. Equivalent water concentrations calculated from this method usually did not replicate, were occasionally negative, and were not consistently within the range of concentrations measured by the direct method. This technique was unsuccessful for several reasons. First, in some houses, low concentrations in bathroom air were difficult to

measure accurately because of residual background activity in the alpha-scintillation cells used to collect the grab samples. Second, in some houses, other, stronger ^{222}Rn sources elevated bathroom air concentrations so that the contribution from the water supplies with low concentrations was overwhelmed. Thus, the calculation involved subtracting one large and uncertain number from another. Table A2 summarizes the data from both measurement methods.

(3) <u>Depressurization by Appliances</u>

The range of additional substructure depressurization due to the operation of various appliances in the houses was difficult to quantify because the pressure differences were small and variable. The variation was usually caused by wind, and the opening of windows, duct registers, and interior doors. In the five houses where pressure differences were monitored as only furnace burners were cycled on/off, the additional depressurization was always less than the 1 Pa detection limit of the portable electronic micromanometer (Table 2). By contrast, in five of the six homes with a forced-air furnace, the blower caused measureable (> 1 Pa) additional depressurization. Air leaks in return plenums and ducts located in the substructure along with substructure supply and superstructure return vents closed by the occupants created this effect.

Although electric fans that exhaust hot air from the attic usually operate only in the summer, they had a surprisingly large impact; lowering basement pressures by almost 17 Pa in house LBL08. The negative pressure developed by the fans is communicated via bypasses (e.g., flue and chimney chases) that connect the attic to the basement. Whole house fans had minimal effect, less than 1 Pa, since windows were usually open during operation of the fan. Clothes dryers (that exhaust to the outside) lowered basement pressures by less than 1 Pa to 2 Pa (see Table A3, Appendix A).

It has been shown that 40 to 90% of the air exhausted by an SSD system may originate in the basement (Turk et al. 1988b). By assuming withdrawal rates of 0.0094 m^3s^{-1} (20 cfm) and 0.0353 m^3s^{-1} (75 cfm), the amount of additional basement depressurization due to operation of SSD systems, which simply adds to the depressurization from other mechanisms (Mowris and

10

Fisk 1987), was calculated for each house using the substructure ELA_b. Only the higher withdrawal rate in houses with tight substructures (LBL11 and LBL12 in Table A4, Appendix A) would cause a significant additional depressurization (-0.5 Pa and -0.2 Pa, respectively).

(4) Soil Air Permeability

Examples of data from the permeability (K) measurements from LBL14C are summarized on Figure 2. Data for the other houses are found in Appendix B. If multiple pressures were used, the permeability at the lowest pressure is presented. The data from all houses ranged from below the minimum detection limit ($\sim 10^{-14}$ m^2) to near the maximum detection limit ($\sim 10^{-8}$ m^2). The measurement values often replicated within a factor of two with the differences attributed to the precision of the measurement system and to changes in soil moisture between measurements. The geometric mean of permeabilities for the soil probes surrounding the houses is approximately 40×10^{-12} m^2 with a geometric standard deviation of 22.1 (Turk et al. 1988b). Permeability measured in the ring of probes placed approximately 0.5 m from the house may be higher due to the less tightly-packed backfill material (Sextro et al. 1988). Permeability values in the gravel below slabs often approached the maximum detection limit (GM of 890×10^{-12} m^2 with a GSD of 16). Permeability values from probes that penetrate into the compacted soil below the subslab gravel layer were much lower (GM of 0.16×10^{-12} m^2 with a GSD of 57). The permeability within 0.01 to 0.02 m of the exterior surfaces of walls was often very high, with a GM of 610×10^{-12} m^2 and a GSD of 8.4.

(5) Blower Door Tests

Measured and calculated effective leakage areas are summarized in Table 3. Whole house ELA_ws varied from house to house by a factor of approximately 3, but the substructure ceiling (ELA_c) and substructure wall/floor (ELA_f) leakage areas varied by a factor of approximately 9. The whole house ELA_w was always smaller than the sum of the substructure and superstructure leakage areas because the latter two each include the leakage of the substructure ceiling, which can be large. In LBL14C, which had the tightest overall building shell, the substructure ceiling had almost twice the leakage of the overall structure. The large leakage area of substructure ceilings can be attributed primarily to holes and openings in the ducts of forced-

air furnaces, but also to combustion appliance flues, and to service penetrations and bypasses to attics. Since the forced-air furnaces were located in the basements of these houses, the return air and fan blower plenum also added significant leakage area. It is instructive to note the low substructure ceiling ELA for house LBL11, which had a hydronic heating system, and therefore, no ducts for air distribution.

Two blower pressurization tests performed on the basement of LBL11 underpredicted the flow rates necessary to overpressurize the basement for Rn control by as much as 40% (Table 4). The predicted flows are compared with flows measured with the overpressurization system in operation at three different pressures. The existing natural depressurization plus the system-induced overpressurization give the total pressure difference (ΔP) that was developed by the fan. The poor prediction of flows using blower door data is probably caused by inaccuracies in measuring the small pressure differences during the blower door test and system operation and in the power curve fitting procedures applied to these data points.

For the first and last measurement dates indicated, the average measured pressure differences across the substructure ceiling were 7.1 Pa and 8.3 Pa respectively. Using these pressure differences and an ELA_c of 0.018 m^2, flow rates from the basement to first floor were calculated to be 0.058 m^{3}s^{-1} (120 cfm) and 0.130 m^{3}s^{-1} (280 cfm). Therefore, for this house, approximately 60% to 85% of the pressurization fan's air flow returned to the upstairs or escaped to the attic through bypasses.

(6) <u>Grab Samples of ^{222}Rn</u>

Radon-222 concentrations for LBL14C are identified on Figure 2 and for the remaining houses in Appendix B by the letter R. Samples from below basement slabs and slabs-on-grade adjacent to a below-grade basement wall usually had the highest ^{222}Rn concentrations for all test locations in or very near the houses. The average concentration for 44 of these locations was 150,000 Bq m^{-3} (with a geometric mean of 43,000 Bq m^{-3} and a GSD of 8.3) and exceeds the average concentration of 18,000 Bq m^{-3} (a GM of 6500 Bq m^{-3} and a GSD of 4.8) for 98 block wall cavities. The wall cavities are probably subjected to greater dilution by outside and house air. Radon-222 concentrations in samples from the indoor test holes at the same house

often ranged from several hundred Bq m^{-3} to over 500,000 Bq m^{-3} (and up to 880,000 Bq m^{-3}).

(7) <u>Vacuum Field Extension</u>

The pressure field developed around the substructure of LBL14C during the test with the industrial vacuum is shown on Figure 3 (the letter V indicates a vacuum test ratio). Appendix C presents data for LBL08, LBL12, and LBL13. While pressure fields extended to greater distances at houses with highly permeable regions or gravel layers around the substructure, the field nonetheless dropped off very quickly with distance from the vacuum hole. An examination of data from all seven houses (Figure A1, Appendix A) showed that the ΔP at 66 floor test holes correlated poorly with distance from the vacuum hole (correlation coefficient, R = -0.23). As observed by other workers, there are inhomogeneities and discontinuities beneath slabs that interrupt distribution of the vacuum pressure field (Gadsby et al. 1988; Fowler et al. 1988; Matthews et al. 1988). Not surprisingly, the pressure field did not extend as effectively to the test holes into and through the block walls. Other researchers have reported on results of more detailed experimental work that characterizes the application of this technique (Mathews et al. 1988; Gadsby et al. 1988).

(8) <u>Pressure Field Mapping and Basement Depressurization</u>

Figure 3 (and Appendices B and C) also displays results of pressure field mapping tests (PFM) conducted at different basement depressurizations. Data from different tests generally replicate well, having a correlation coefficient of 0.79. The mean coupling ratio for 161 indoor test holes was 0.35 with a standard deviation (SD) of 0.29 (and a median of 0.30). In particular, the average coupling ratio for 85 holes into block wall cavities was lower (0.25 with a SD of 0.25 and a median of 0.20) than that for 38 holes into the gravel below the slab (0.39 with a SD of 0.22 and a median of 0.30), or for 27 holes into soils below the gravel layer or along wall exteriors (0.48 with a SD of 0.35 and a median of 0.50). This implies that the interior of the block walls have a better coupling, through openings, leakage pathways, or their porous surfaces, to the interior of the basement than the other spaces surrounding the substructure.

Air velocities and pressure differences between the end of the test holes and the basement interor were compared for tests at different basement pressures. Velocities up to 2.5 m s^{-1} were measured in the flow adaptor during basement depressurization of 30 Pa. In general, velocities varied almost linearly with increasing ΔP. However, a number of floor and wall holes had unusually low velocities possibly due to low permeability materials at the ends of the holes (Figure A2, Appendix A). In two houses, pressure differences and velocities were measured at 22 test holes at several basement pressures. Velocities through test holes did not increase exactly in direct proportion to the ΔP across the test holes. A flow exponent, n, was calculated for each of the 22 test holes from

$$Q_2/Q_1 = [\Delta P_2/\Delta P_1]^n, \tag{5}$$

where:

Q_1, ΔP_1 =   first flow and ΔP, respectively, and

Q_2, ΔP_2 =   second flow and ΔP, respectively.

This calculation is strictly valid only if the pressure difference across the test holes did not change appreciably when the test holes were opened to perform the flow measurements. The average value of n for these test holes was 0.92; however, the SD of 0.69 is large. The large standard deviation could result from inaccuracies in the measured velocities and pressures or from irregularities in the size and shape of the holes and hole openings. This result suggests that errors can be expected from attempts to measure permeability (assuming linear Darcy flow) through test holes into porous materials adjacent to substructures (soils, gravels, etc.).

To determine if trained technicians could use the relative flow rate of chemical smoke to accurately represent the air velocity at test holes, smoke flow data was coded and compared against measured flow velocities (Figure A3, Appendix A). Codes were from 0 (no movement observed) to 5 (very rapid movement). These codes appear to be a crude indicator of velocity that is affected by the perception of volumetric flow at holes of different size. At low velocities, the qualitative description using smoke is roughly proportional to velocity, but the technicians could not differentiate between velocities larger than approximately 0.4 m s^{-1}. However, flow detection with smoke is much more sensitive than velocity and ΔP

measurements and is, therefore, still a useful tool.

During 30 Pa depressurization of the basements in four houses, chemical smoke was used to detect air movement at soil grade along the exterior of substructure walls where the soil meets the wall. At every house, there was at least one location where the smoke was pulled into the gap of varying width between the house and soil. At house LBL08, smoke was also drawn into soil cracks and small depressions in the soil (approximately 0.07 m in diameter and unknown depth) near downspouts that were within 0.3 m of the substructure walls. Presumably, openings in the substructure surfaces permitted the low pressure in the basement to pull outside air into these high permeability pathways near the building.

Velocities measured at the test holes during vacuum field tests and pressure field mapping were compared in an attempt to relate the two diagnostic procedures (Figure A4, Appendix A). There was poor correspondence between the two velocities, probably due to the differences in the point(s) where the low pressure was applied.

DISCUSSION AND ANALYSIS

The visual inspection and tour of the building is an essential, if not the most important, task prior to selecting, designing, and installing a Rn control system. This inspection can quickly direct an investigator to the important factors causing high indoor ^{222}Rn levels and the solutions that are mostly likely to reduce those levels. In buildings where construction materials are suspected of contributing significant ^{222}Rn into the indoor atmosphere, the relatively simple, short-term test with charcoal canisters appears to be useful, although none of the houses studied here exhibited problems related to materials.

The alternative technique for determining ^{222}Rn-in-water concentrations by collecting grab samples of bathroom air is not recommended because of large uncertainties in measuring low ^{222}Rn concentrations (or small changes in concentration). Improvements to this technique, including more care in maintaining low backgrounds in the alpha-scintillation cells, longer counting of cell activity, using a more appropriate transfer coefficient, and operating the shower for a longer period may result in more precise and accurate measurements.

15

By measuring the additional depressurization caused by certain appliances that operate for extended periods, solutions can be devised to eliminate or minimize this effect. According to data from these houses, attic exhaust fans can cause the greatest increase in basement depressurization, however the longer operating times of forced-air system blowers may result in more persistent additional depressurization exacerbating the forces drawing Rn-bearing soil gas into buildings. In addition, where these systems have leaky return air ducts and plenums or open return air vents in the substructure, the high ^{222}Rn concentration substructure air is distributed more readily throughout the remainder of the building (Harrje et al. 1989; Revzan et al. 1987; Turk et al. 1988b).

Blower door tests were useful for comparing the air leakage of different building zones, and identifying tightly-sealed substructures so that basement pressurization may be considered as a control system option. Although the blower door did not accurately predict the actual flow rates measured during operation of a basement pressurization system, the predictions may be satisfactory for evaluating the feasibility of this technique. To apply the predictions correctly, the natural depressurization at the basement floor that is induced by maximum indoor-outdoor temperature differences must be estimated from the structure height and climatological data. A minimum overpressurization of 2 Pa to 3 Pa is then added to the estimated natural depressurization and the required flows are calculated at that total pressure difference. The substructure ceiling and wall/floor leakage area measurements can indicate where additional attention to sealing is necessary to reduce the flow rates required for overpressurization and reduce the energy penalty associated with the loss of conditioned air.

Soil air permeability measurements show the presence of very high permeability regions adjacent to exterior surfaces of substructures. These regions probably consist of gravel, loosely packed backfill material, and air gaps caused by expansion/contraction cycles and settling. Although these regions may result in higher original (pre-mitigation) flow rates of ^{222}Rn into the structure, they may also furnish a high permeability pathway that extends the pressure field and effectiveness of SSV Rn control systems (provided that these regions are continuous and not interrupted by impermeable barriers). This technique, along with the collection of soil

samples, has furnished useful research information, but is not essential for the private contractor.

Soil Gas and ^{222}Rn Entry Potentials

While none of the procedures associated with the pressure field mapping and vacuum field extension tests can provide foolproof guidance for the design of SSV mitigation systems and a guarantee of the eventual long-term effectiveness of these systems, some of the data from the field measurements may be used to develop parameters that quantify (approximately) the potential for soil gas and ^{222}Rn to enter a building at different locations. The low coupling ratios indicate regions surrounding substructures that, in some way, have good connection to the interior of the substructure. By itself, good coupling of the pressure field to a test hole location does not confirm that large quantities of soil gas enter the building through nearby openings. The soil, aggregate, or backfill material around the substructure must also be sufficiently permeable so that substantial soil gas can be transported to the openings. Therefore, a location near the substructure with good pressure coupling to the interior of the substructure and with a relatively high flow through a test hole is a likely entry location for significant quantities of soil gas. There are many such regions near houses as indicated by measured high values of permeability, high velocities measured at test holes during pressure field mapping tests, and by the observation of air movement along the below-grade surfaces of exterior walls caused by the ΔP in the substructure.

The passage of soil gas into a substructure depends upon the flow path resistances through the materials surrounding the substructure and through the surfaces of the substructure. A simplified electrical analog of the house-soil system can be created to simulate the flows, pressure drops, and resistances in the soils, near-house materials, and substructure surfaces (Figure 4a and b). Two measurement conditions are shown: the test hole sealed, and the test hole open (indicated by dotted lines representing the flow, I_H, and resistance, R_H, of the test hole and flow adaptor). Following are definitions and the corresponding electrical parameters (use of the subscript 'C' with any of these terms identifies the condition with the test hole closed):

17

Q_H (I_H) = measured (corrected) flow through open test hole and flow adaptor (m^3s^{-1}),

Q_F (I_F) = flow through cracks and openings in below-grade substructure surfaces with test hole open (m^3s^{-1}),

Q_T (I_T) = total flow through cracks, openings, and open test hole (m^3s^{-1}),

P_B (V_B) = measured pressure difference between inside of basement and outside, point a to c (Pa),

P_H (V_H) = calculated pressure drop across open test hole and flow adaptor, point a to b (Pa),

P_S (V_S) = pressure drop across soil paths between point b and outside with test hole open (Pa),

R_H = resistance of open test hole and flow adaptor (Pa-s/m^3),

R_{F-EFF} = calculated effective resistance that lumps resistances of cracks and openings in substructure surfaces and resistances of near-surface materials surrounding the open test hole (R_{F1}, R_{F2}, R_{F3}, etc.) (Pa-s/m^3), and

R_{S-EFF} = calculated effective resistance of soil paths to measurement point b (R_{S1}, R_{S2}, R_{S3}, etc.), with test hole open (Pa-s/m^3).

No velocity corrections were made based on test hole size or configuration. These corrections are estimated to have been less than ±10%. Drilling all holes to the same diameter is the preferred alternative. To compute the volumetric flow rates, we used the measured velocities and the cross-sectional area of the flow adaptor minus the projected area of the hot wire anemometer probe. For pressure differences and flow rates that were below detection limits, values of 0.5 times the detection limit were assumed. Final results are insensitive to this assumption.

Pressure drops across the flow adaptor and test hole (P_H) were estimated using the engineering formula for laminar flow through a tube

$$-\frac{dP_H}{dx} = \frac{8\mu Q_H}{\pi r^4} \quad ,$$

[6]

where P_H = pressure drop (Pa),
                x = length of test hole plus flow adaptor (m),
                μ = absolute viscosity of air, 1.8×10^{-5} kg/m-s, and
                r = radius of the tube (in our case, we used the radius of the flow adaptor of 0.0045 m).

Estimated pressure drops ranged from less than 0.01 Pa to 3.5 Pa. In theory, a more accurate value for this pressure drop could be determined by direct measurement; however the small pressure differences are difficult to measure in practice.

We assume that the complex network of resistances through the soil and substructure surfaces can be represented approximately by the simplified circuit shown to the left in Figure 4b. With the test hole sealed, a resistance ratio (Z), i.e., the resistance of the substructure surfaces and near-surface materials divided by the resistance of the soil, can be defined as

$$Z = \frac{V_{HC}}{V_{SC}} = \frac{I_{TC} R_{FC\text{-}EFF}}{I_{TC} R_{SC\text{-}EFF}} = \frac{R_{FC\text{-}EFF}}{R_{SC\text{-}EFF}} \quad , \text{ thus} \qquad [7]$$

$$R_{FC\text{-}EFF} = Z(R_{SC\text{-}EFF}). \qquad [8]$$

When the test hole is open, the following three independent equations are derived

$$V_B - I_H R_H - I_T R_{S\text{-}EFF} = 0, \qquad [9]$$

$$I_F R_{F\text{-}EFF} - I_H R_H = 0, \text{ and} \qquad [10]$$

$$I_T - I_F - I_H = 0. \qquad [11]$$

If we assume that

$$R_{FC\text{-}EFF} \sim R_{F\text{-}EFF} \text{ and}$$

$$R_{SC\text{-}EFF} \sim R_{S\text{-}EFF}$$

then we can solve for $R_{S\text{-}EFF}$, using equations 8 through 11 and substituting for analogous parameters, to obtain

$$R_{S\text{-}EFF} = \frac{P_B - P_H \dfrac{1}{1 + Z}}{Q_H} \quad . \qquad [12]$$

$R_{F\text{-}EFF}$ can be determined from equation 8.

19

The calculated effective resistances for 117 test holes (including some replicates) are summarized on Table 5. The data are highly variable as indicated by the large standard deviations. However, by examining the geometric means, several patterns are apparent: (1) the effective soil resistance that is 'seen' by test locations in slab floors and block cavities is similar, probably because large surface areas of soil (and for the block walls - areas exposed directly to the outside) are accessible by these holes, (2) the slab floors are approximately five times more resistant to soil gas movement than the porous block walls, and (3) for all locations, except those in the soil exterior to the walls, the substructure 'sees' the soil as being a factor of 2 to 7 more resistant to soil gas flow than the substructure surfaces and materials very near to the substructure.

We can define the entry potential (net conductance) for soil gas, G $(m^3/Pa-s)$, from

$$I_T = \frac{V_B}{R_{S-EFF} + R_{F-EFF}} \text{, or} \tag{13}$$

$$G = \frac{1}{R_{S-EFF} + R_{F-EFF}} \propto Q_T \tag{14}$$

Values of G ranged from less than 0.01×10^{-6} $m^3/Pa-s$ to 3.2×10^{-6} $m^3/Pa-s$. The data for LBL14C are plotted on Figure 3 and for LBL08, LBL12, and LB13 on Figures C1-C3, Appendix C. These figures and data from all four houses in Table 6 show that the soil gas entry potentials for the hollow-core block walls are higher than for the other locations probably because of the lower effective resistance of the block material and the large exterior surface area of wall exposed to soil and/or outdoor air. Note that the relative standard deviations (RSDs) were much smaller for those test locations bordered by high permeability regions -- gravel below slabs or open block cavities -- than for locations immediately adjacent to the exterior of the walls.

The soil gas entry potential at a particular location is affected by all soils, materials, and openings in the surfaces around a building, but more so by those nearby or connected by a high permeability path. More study is required to determine the distance from a test hole over

which the soil gas entry potential is applicable. When this relationship is better understood, the test holes can be better placed to best represent the soil gas entry throughout the entire substructure.

To describe the potential for ^{222}Rn entry into a building at a location, another parameter is necessary. This number, the ^{222}Rn entry potential, E (Bq/Pa-s), can be defined by multiplying the soil gas entry potential by the ^{222}Rn concentration, C (Bq m^{-3}), in a grab sample of air collected from the test hole:

$$E = GC \quad .$$

[15]

Thus, the ^{222}Rn entry potential should indicate the likelihood that significant amounts of ^{222}Rn can enter a substructure at a particular location. In this study, grab samples were not always collected from the test holes concurrently with the measurements of flow and pressure drop. Therefore, ^{222}Rn concentrations from grab samples collected at other times were averaged and used to compute the ^{222}Rn entry potential. The data are summarized on Figure 3 (and Figures C1-C3) and on Table 6. For a similar set of 73 holes in four houses the geometric mean ^{222}Rn entry potential was, on average, highest for the test holes into the subslab aggregate. Although the block wall test holes had a slightly higher soil gas entry potential, the subslab test holes had greater concentrations of ^{222}Rn in the soil gas which compensated for their smaller soil gas entry potential. Calculated values of E ranged from less than 0.1×10^{-3} Bq/Pa-s to 1300×10^{-3} Bq/Pa-s.

When ^{222}Rn entry potential data are plotted on plans of all four houses, similar to Figure 3, we find that the areas of highest ^{222}Rn entry potential generally coincide with the locations where pipes of successful SSD systems were placed through the slabs. For these houses, a 'high' ^{222}Rn entry potential would be considered greater than approximately 15×10^{-3} Bq/Pa-s. Since the entry potentials were calculated after installation of the SSD systems, these indices appear to provide a quantitative method for replicating the intuitive approach of successful mitigation contractors. LBL12 is an exception, where it was difficult to bring indoor ^{222}Rn levels below the target of 148 Bq m^{-3}. A review of the data from this house indicates areas of high ^{222}Rn entry potential that were not in proximity to an SSD pipe, and may have been the

21

sources of inadequately controlled Rn entry (Figure C2, Appendix C).

In general, the ^{222}Rn entry potential indicates the preferred locations for SSD pipes, but does not provide information about the ability of a specific SSV system to reduce ^{222}Rn entry rates. The vacuum test remains the best technique to measure the extent to which a SSD system can reverse the natural pressure gradient around a substructure, and therefore control ^{222}Rn entry. Therefore, combining the vacuum test with identified areas of high ^{222}Rn entry potentials can benefit decisions for placement of SSV pipes. When the soil gas entry potential is high, but communication or connection to the vacuum location is poor for a particular test point, obstructions or high permeability short circuits are probably blocking or intercepting the extension of the pressure field from the vacuum. The problem is then to provide access to the areas of high ^{222}Rn entry potential.

The geometric mean of the ^{222}Rn entry potentials for each of the four houses was compared with the average indoor ^{222}Rn concentration, measured between September 1 and May 1, and weighted by the volumes for various zones where indoor ^{222}Rn was measured. From the lowest to highest ^{222}Rn concentration; 540, 620, 650, and 660 Bq m^{-3}, the geometric mean ^{222}Rn entry potentials were 6.4, 10, 7.2, and 18 $\times$ 10^{-3} Bq/Pa-s, respectively. For the third house listed (LBL13), the GM ^{222}Rn entry potential fails to trend with increasing indoor ^{222}Rn concentrations and suggests weaknesses in the current development or application of the new parameters.

For example, the assumptions, $R_{FC-EFF} = R_{F-EFF}$ and $R_{SC-EFF} = R_{S-EFF}$, are not exactly valid, since the paths for air flowing through the soil and building surfaces are different in the two measurement conditions. The effects of inhomogeneities, in soils, and near-house and substructure surface materials on the assumption have not been examined. The derivation is also sensitive to the calculated pressure drop across the test hole and flow adaptor (P_H), which could easily be in error by a factor of two. Although a larger substructure-outside pressure difference (P_B) developed by the blower door does not simulate actual house operating conditions, it does increase the magnitude of most parameters so that they can be more easily measured. By artificially depressurizing the building, many seasonal effects can be minimized

22

and another short-term test that is being evaluated can be conducted simultaneously to simulate winter indoor radon concentrations.

Summarizing this section, two new parameters have been defined, based upon easily obtained data. These parameters are imperfect but useful to: (1) identify areas in a substructure with the potential for comparatively high soil gas entry rates; (2) compare the relative leakiness of below-grade surfaces in different houses; (3) provide approximate measures of the resistance of substructure surfaces and soils/materials around the substructure; (4) identify areas in a substructure with potentially high ^{222}Rn entry rates for placement of radon control systems; and (5) provide a basis for establishing the relative importance of substructure and soil characteristics to ^{222}Rn entry.

REFERENCES

Brennan, T.M. et al. Reducing indoor radon: A training manual (Second Edition), Albany, NY:

New York State Energy Office; 1988.

DSMA Atcon Ltd. Review of existing instrumentation and evaluation of possibilities for research and development of instrumentation to determine future levels of radon at a proposed building site. Ottawa, Canada: Atomic Energy Control Board; Report INFO-0096; 1983.

Fowler, C.S.; Williamson, A.D.; Pyle, B.E.; Belzer, F.E.; Sanchez, D.C.; and Brennan, T.M. Sub-slab depressurization demonstration in Polk County, Florida, slab-on-grade houses. Proceedings of U.S. EPA 1988 Symposium on Radon and Radon Reduction Technology; Paper VII-6; Denver, CO; 1988.

Gadsby, K. J.; Hubbard, L.M.; Harrje, D.T.; and Sanchez, D.C. Rapid diagnostics: subslab and wall depressurization systems for control of radon. Proceedings of U.S. EPA 1988 Symposium on Radon and Radon Reduction Technology; Paper VI-P1; Denver, CO; 1988

Gesell, T.F. and Prichard, H.M. The contribution of radon in tap water to indoor radon concentrations. In: Proceedings of the symposium on the natural radiation environment III. U.S. Department of Energy, CONF-80422; Springfield, VA: NTIS 2: 1347-1363; 1980.

Harrje, D.T.; Hubbard, L.M.; and Sanchez, D.C. Proceedings of the radon diagnostics workshop. Princeton University: CEES Report No. 223; 1987.

Harrje, D.T.; Hubbard, L.M.; Gadsby, K.J.; Bolker, B.; and Bohac, D.L. The effect of radon mitigation systems on ventilation in buildings. ASHRAE Transactions. 95: part 1; 1989.

Matthews, T.G.; Wilson, D.L.; TerKonda, P.K.; Saultz, R.J.; Goolsby, G.; Burns, S.E.; and Haas, J.W. Radon diagnostics: subslab communication and permeability measurements. Proceedings of the Symposium on Radon and Radon Reduction Technology, Paper VI-4; U.S. EPA, Denver, CO; 1988.

Mowris, J.J. and Fisk, W.J. Modeling the effects of exhaust ventilation on radon entry rates and indoor radon concentrations. Health Physics. 54:5,491-501; 1987.

Nazaroff, W.W.; Doyle, S.M.; Nero, A.V.; and Sextro, R.G. Potable water as a source of airborne radon-222 in U.S. dwellings: A review and assessment. Health Physics; 3:52:281-295; 1985.

Nazaroff, W.W.; Lewis, S.R.; Doyle, S.M.; Moed, B.A.; and Nero, A.V. Experiments on pollutant transport from soil into residential buildings by pressure-driven air flow. Environmental Science and Technology;21:459; 1986.

Nero, A.V. and Nazaroff, W.W. Characterizing the source of radon indoors. Radiation Protection Dosimetry; 7:23-29; 1986

Revzan, K.L.; Turk, B.H.; Harrison, J.; Nero, A.V.; Sextro, R.G. Parametric modeling of temporal variations in radon concentrations in homes. IEEE Transactions on Nuclear Science; 35(1):550-555; 1987.

Sanchez, D.C.; Hubbard, L.M.; Harrje, D.T.; and Turk, B.H. The use of diagnostic measurements to enhance the selection and effectiveness of radon mitigation for detached dwellings. In: Proceedings of the 4th international conference on indoor air quality and climate, institute for water, soil and air hygiene. Berlin: 1982:370-375.

Sextro, R.G.; Nazaroff, W.W.; and Turk, B.H. Spatial and temporal variations in factors governing the radon source potential of soil. Proceedings of the Symposium on Radon and Radon Reduction Technology; Paper V-5, U.S. EPA, Denver, CO; 1988.

Turk, B.H.; Harrison, J.; Prill, R.J.; Sextro, R.G. Interim report on diagnostic procedures for radon control. Report No. LBL-23089; Berkeley, CA: Lawrence Berkeley Laboratory; 1987a.

Turk, B.H.; Prill, R.J.; Fisk, W.J.; Grimsrud, D.T.; Moed, B.A.; Sextro, R.G. Radon and remedial cction in Spokane River Valley homes. Volume 1: experimental design and data analysis. Berkeley, CA: Lawrence Berkeley Laboratory; Report No. LBL-23430; 1987b.

Turk, B.H.; Harrison, J.; Sextro, R.G.; Hubbard, L.M.; Gadsby, K.J.; Matthews, T.G.; Dudney, C.S.; and Sanchez, D.C. Evaluation of radon reduction techniques in fourteen basement houses: preliminary results. In: Proceedings of the 81st annual meeting of the air pollution control association. Dallas, TX, 88-107.2; Berkeley, CA: Lawrence Berkeley Laboratory; Report No. LBL-25127; 1988a

Turk, B.H.; Harrison, J.; Prill, R.J.; and Sextro, R.G. Intensive radon mitigation research:

lessons learned. Proceedings of the symposium on radon and radon reduction technology; Paper VI-3; U.S. EPA, Denver, CO; 1988b

Table 1. Key to Symbols for Figures 2 and 3

___

<u>LOCATIONS</u>

I = Indoor
  W = Wall
      (B) = Into block wall cavities
      Blank = Through wall into soil
      Top = Opening at top of wall
  F = Through floor

O = Outdoor
  A = ~0.5 m from house
  B = ~1.5 m from house
  C = ~3.0 m from house
  N,E,W,S = Orientation to compass direction
1,2,3,... = Arbitrary sample location number

<u>MEASUREMENTS</u>

PFM = Pressure field map coupling ratio $\left(\dfrac{\Delta P_{TESTHOLE}}{P_{OUTSIDE} - P_{BASEMENT}} \right)$

      I = Initial test, basement depressurized to -30 Pa
      10 = Basement depressurized to -10 Pa
      30 = Basement depressurized to -30 Pa
      OR = Over range
K = Permeability ($\times 10^{-12}$ m^2)
R = ^{222}Rn concentration ($\times 1000$ Bq m^{-3})
      (Dates)   S = 9/86
                 O = 10/86
                 M1 = First 5/87 test
                 M2 = Second 5/87 test
                 J1 = First 6/87 test
                 J2 = Second 6/87 test
                 J3 = Third 6/87 test
                 D = Diagnostic test

V = Vacuum test ratio $\left(\dfrac{\Delta P_{TESTHOLE}}{\Delta P_{VACUUMHOLE}} \times 10^{-3} \right)$

G = Soil gas entry potential ($\times 10^{-6}$ m^3/Pa-s)
E = ^{222}Rn entry potential ($\times 10^{-3}$ Bq/Pa-s)

___

Table 2. Additional Depressurization due to Appliance Operation

Additional Bsmt. Depress.* (Pa)	(No. of Houses)					
	Furnace Burner Only	Furnace Blower Only	Furnace Burner + Fan	Clothes Dryer	Whole House Fan	Attic Fan
< -1	5	0	1	1	0	0
< -1 to -2	0	2	1	1	1	0
-2 to -4	0	1	1	1	0	1
-4 to -6	0	0	1	0	0	1
-6 and greater	0	1	0	0	0	1
Total No.	5	4	4	3	1	3

* Ranges of additional depressurization include the ranges observed to occur at each house. For example, various duct register openings at LBL12 caused the additional depressurization to range from <-1 to -1.5 Pa.

Table 3. Effective Air Leakage Areas (ELA)

	[m² (no. of measurements)]				
House ID	Whole house (ELA_w)	Substructure (ELA_b)	Superstructure (ELA_p)	Substructure ceiling (ELA_c)	Substructure walls/floor (ELA_f)
8	0.17	0.28	0.19	0.15	0.13
9	0.14(3)	0.13(3)	0.13(3)	0.061	0.073
10	0.14(2)	0.16	0.22	0.12	0.043
11*	0.087(2)	0.041	0.081	0.018	0.024
12*	0.078	0.068	0.12	0.053	0.015
13	0.12	0.14	0.20	0.11	0.026
14	0.06	0.13	0.14	0.10	0.023

* After air-leak tightening of basement for installation of basement pressurization Rn control system.

Note: Unless otherwise indicated, only one measurement was used.

Table 4.   Comparing Measured and Blower Door Predicted Flow
Rates for Basement Pressurization System at LBL11

| | Measurement Dates | | |
	February 12	March 21	March 30
Pressurization Fan Boosted ΔP (Pa)	3.8	4.9	5.7
Pressurization Fan Measured Flow (m^3s^{-1})	0.10	0.15	0.15
Blower Test (Feb. 10) Predicted Flow (m^3s^{-1})	0.10	0.13	0.14
Blower Test (Mar. 20) Predicted Flow (m^3s^{-1})	0.071	0.93	0.11

Table 5. Statistical Summary of Effective Resistances for Soils and Substructure Surfaces
from Four Houses

Material Category	Below Slab Gravel	Block Wall Cavity	Exterior to Wall	All Locations
		Test Hole Location		

Soils, R_{S-EFF} ($\times 10^6$ Pa-s/m^3)

	Below Slab Gravel	Block Wall Cavity	Exterior to Wall	All Locations
Geom. Mean	1.1	0.78	2.6	10
Geom. Std. Dev.	5.1	2.5	5.4	3.7
Median	0.58	0.71	1.6	0.73
Arith. Mean	5.7	1.6	8.5	3.6
Arith. Std. Dev.	13	3.8	14	9.4
Number	33	69	15	117

Surfaces, R_{F-EFF} ($\times 10^6$ Pa-s/m^3)

	Below Slab Gravel	Block Wall Cavity	Exterior to Wall	All Locations
Geom. Mean	0.55	0.11	4.6	0.28
Geom. Std. Dev.	5.1	2.5	7.9	6.3
Median	0.43	0.11	4.7	0.18
Arith. Mean	2.7	0.16	18	3.1
Arith. Std. Dev.	6.8	0.19	29	12
Number	33	69	15	117

Table 6. Statistical Summary of Soil Gas and Radon Entry Potentials from Four Houses

Potential	Below Slab Gravel	Block Wall Cavity	Exterior to Wall	All Locations
		Test Hole Location		

Soil Gas Entry Potential ($\times 10^{-6}$ m^3/Pa-s)

Potential	Below Slab Gravel	Block Wall Cavity	Exterior to Wall	All Locations
Geom. Mean	0.5	1.2	0.11	0.73
Geom. Std. Dev.	4.8	1.6	4.3	3.6
Median	1.2	1.3	0.17	1.2
Arith. Mean	1.1	1.4	0.24	1.1
Arith. Std. Dev.	0.85	0.52	0.28	0.70
Number	22	44	9	75

Radon-222 Entry Potential ($\times 10^{-3}$ Bq/Pa-s)

Potential	Below Slab Gravel	Block Wall Cavity	Exterior to Wall	All Locations
Geom. Mean	23	7.9	3.2	9.7
Geom. Std. Dev.	6.7	5.1	6.4	6.2
Median	31	8.1	3.4	11
Arith. Mean	110	24	21	48
Arith. Std. Dev.	280	42	54	160
Number	22	42	9	73

Figure 1   Flow adaptor device used to measure flows through test holes during various tests. The bottom opening of the adaptor seals against the test hole surface, while flows are measured with a hot wire anemometer probe placed inside the open tube of the adaptor. Dimensions are in millimeters.

Figure 2   A site plan of house LBL14C that shows the locations of probes in the soil around the house, holes drilled through the slab floors (solid dots), and of test holes drilled into and through hollow block walls (vertical and horizontal lines). Measured data for soil air permeabilities (K), and ^{222}Rn grab samples (R) are mapped with the identification of the test hole. See Table 1 for more complete descriptions of the codes that are used.

Figure 3   Similar to Figure 2, except that data for coupling ratios during pressure field mapping tests (PFM), vacuum field extension tests (V), soil gas entry potentials (G), and ^{222}Rn entry potentials (E) are mapped. The single SSD pipe penetrated the slab along the east wall. The pressure difference at the vacuum hole location during testing was -770 Pa.

Figure 4   Drawing of substructure during pressure field mapping and basement depressurization (a). A simplified electrical analog of the various flows, pressure drops, and resistances during the test depicted in (a) is shown in (b). The dotted line indicates the variables associated with an open test hole. A further simplification is shown by the circuit on the left side of (b).

Figure 1

PROFILE

←— 26 —→

—→ 9 ←—

100

← FLOW
  ADAPTOR

OPEN
FLOW TUBE

SILICONE
GASKET

TEST
HOLE

HOT WIRE
ANEMOMETER
PROBE

TOP VIEW

Figure 2

N

OCN1 ●

OCN2 ●

● OCN3
R(M1)= 56
R(M2)= 110
R(J1)= 135
R(J3)= 34

OBN1
K(S)= 70
K(O)= 64
R(S)= 130

● OAN4
K(S)= 47
R(S)= 98
R(M1)= 100
R(M2)= 53
R(J1)= 110
R(J3)= 83

OBN2
K(S)= 1200
K(O)= 1200
R(S)= 130
R(O)= 150
R(M1)= 120
R(M2)= 140
R(J1)= 150
R(J3)= 72

OAN1
K(S)= 21
K(O)= 64

● OAN2
K(S)= 96
R(S)= 52
R(O)= 42

● OAN3
K(S)= 36
R(S)= 37

● OAE1
K(S)= 33
R(O)= 46

OCW1
●

OAW1
K(S)= 620
R(O)= 58
R(M1)= 120
R(M2)= 48
R(J1)= 120
R(J3)= 47

IW3
K(S)= 15
R(S)= 22
R(D)= 26

IW13(B)
R(D)= 1.8
R(J2)= 1.9

IW13Top
R(D)= 2.5

IW4
R(D)= 34

IW5(B)
R(D)= 17

IF5
R(D)= 140
R(J2)= 99

● OCE1

IF4
R(D)= 4.2
R(J2)= 38

IF3
R(D)= 14
R(J2)= 9.5

OBE1
K(S)= 0.92
K(O)= 0.75
R(S)= 100
R(O)= 61

IW12(B)
R(D)= 0.7

IW11(B)
R(D)= 2.5

VAC. HOLE

GARAGE

IF1
R(S)= 85
R(D)= 78

IF2
K(S)= BD
R(S)= 47
R(D)= 12

IW6Top
R(D)= 8.9

● OAE2
K(S)= 150
R(S)= 53
R(O)= 35

OTHER DIAGNOSTICS DATA

Ambient Air Samples (Bq/m³)

Diagnostics (6/8-9/87)

Basement   400
Level 1 Liv Rm   50
Level 2 Bedroom   300

Flux Measurements (Bq/m²-s)

8/28/87

N Wall Center   0.0009
N Wall Center   0.0014

Water Samples (Bq/m³)

8/10/87   51,000

IW10(B)
R(D)= 1.4
R(J2)= 0.4

BASEMENT

IW6(B)
R(D)= 15
R(J2)= 4.3

IW1
K(S)= 75
R(S)= 39
R(D)= 82

IW7Top
R(D)= 36
R(J2)= 14

IF9
R(D)= 1.0

IW9Top
R(D)= 1.4

IF6
R(D)= 110
R(J2)= 110

IF8
R(D)= 0.8

IW9Top
R(D)= 0.04

BSMT. ANNEX

IW7(B)
R(D)= 46

IF7
R(D)= 9.1

● OAE3
K(S)= BD
R(S)= 4.1

IW2
K(S)= 62
R(D)= 40

IW8(B)
R(D)= 6.7

● OAS2
K(S)= 310
R(S)= 61
R(O)= 58
R(M1)= 42
R(M2)= 43
R(J1)= 59
R(J3)= 44

● OAS1
K(S)= 200
R(S)= 58

OCS2
R(M1)= 84
R(M2)= 70
R(J1)= 86
R(J3)= 75

OCS1

●   ●

9.8'

Figure 3

Figure 4(a)

4(b)

APPENDIX A

This appendix contains tables and figures of summary data that are discussed in the text.

Table A1. Building Material Surface Flux Measurements

House ID	Test Start Date	Location	Flux (Bq/m^2-s)	Rn Entry (Bq/s)	Volume Normalized Source Rate (Bq/m^3-s)
8	31-OCT-86	W basement floor	0.023	3.2	0.0034
8	31-OCT-86	W end S wall	0.0095	0.62	
9	03-NOV-86	basement floor	0.015	0.77	0.0041
9	03-NOV-86	E crawlspace floor	0.0009	0.057	
9	03-NOV-86	E crawlspace wall	0.049	2.2	
9	03-NOV-86	W crawlspace floor	0.0020	0.014	
10	29-OCT-86	NW family room floor	0.014	0.57	0.074
10	29-OCT-86	W basement floor	0.012	0.90	
10	29-OCT-86	W basement wall	1.9	27	
10	28-AUG-87	center E wall	0.47	11	
10	28-AUG-87	S end E wall	0.3	6.7	
11	02-NOV-86	center basement floor	0.0048	0.38	0.0036
11	02-NOV-86	S end W wall	0.19	2.2	
12	01-NOV-86	center basement floor	0.0066	0.40	0.015
12	01-NOV-86	center crawl floor	0.019	0.36	
12	01-NOV-86	E basement wall	0.12	7.2	
13	04-NOV-86	center S wall	0.0068	0.065	0.0041
13	04-NOV-86	SW basement floor	0.036	2.2	
13	27-AUG-87	center S wall high	0.019	0.19	
13	30-AUG-87	center S wall	0.013	0.12	
13	30-AUG-87	center S wall high	0.010	0.10	
14	28-AUG-87	center N wall	0.0009	0.038	0.0023
14	28-AUG-87	central N wall	0.0014	0.059	
14		floor (estimate)	0.013	1.2	

Table A2. Radon-in-Water Concentrations from Shower Tests and Gamma Spectrometric Analysis of Samples

House ID	Shower Test Date	Shower Test Equivalent Rn-in-Water Concentration (Bq/m³)	Water Grab Sample Date	Water Sample Concentration (Bq/m³)
8	31-OCT-86	270000	05-NOV-86	310000
8	15-APR-87	-39000	09-AUG-87	140000
8	04-MAY-87	-560000		
8	26-JUN-87	290000		
9	03-NOV-86	-7000	05-NOV-86	4500
9	26-JUN-87	-4700	04-AUG-87	10000
10	30-OCT-86	17000	31-OCT-86	8100
10	05-MAY-87	-23000	04-AUG-87	46000
10	30-JUL-87	32000		
11	02-NOV-86	-200000	04-NOV-86	9000
11	12-JUN-87	7100	09-AUG-87	17000
12	01-NOV-86	25000	03-NOV-86	31000
12	04-MAY-87	41000	10-AUG-87	39000
12	28-JUN-87	8400		
13	04-NOV-86	26000	05-NOV-86	4100
13	30-JUN-87	1300	04-AUG-87	12000
13	31-JUN-87	-9800		
14	08-JUN-87	18000	10-AUG-87	51000
14	27-JUL-87	-30000		

Table A3. Additional Depressurization Due to Appliance Operation

| Additional Depressurization (Pa)* | (No. of Houses) | | | | | |
	Furnace Burner Only	FAF Fan Only	FAF Burner & Fan	Clothes Dryer	Whole House Fan	Attic Fan
< -1	5	0	1	1	0	0
≤ -1 to < -2	0	2	1	1	1	0
-2 to < -4	0	1	1	1	0	1
-4 to < -6	0	0	1	0	0	1
-6 and greater	0	1	0	0	0	1
Total no. of houses	5	4	4	3	1	3

*Pressure difference measured between basement interior at height of floor and outside

Table A4. Estimated Additional Basement Depressurization due to Subsurface Depressurization (SSD)

House ID	ELA$_b$ Upstairs Open (cm^2)	Additional Basement Depressurization (Pa) @ 34 m^3/h	Additional Basement Depressurization (Pa) @ 127 m^3/h
8	2800	0.001	0.01
9	1300	0.003	0.04
10	1600	0.002	0.02
11	410	0.032	0.45
12	680	0.011	0.16
13	1400	0.003	0.04
14	1300	0.003	0.05

PRESSURE FIELD DISTRIBUTION DURING VACUUM TEST
Only Positive Pressure Values

Pressure Difference (Pa)

Distance from Vacuum Hole (m)

● Floor Holes
○ Wall Holes
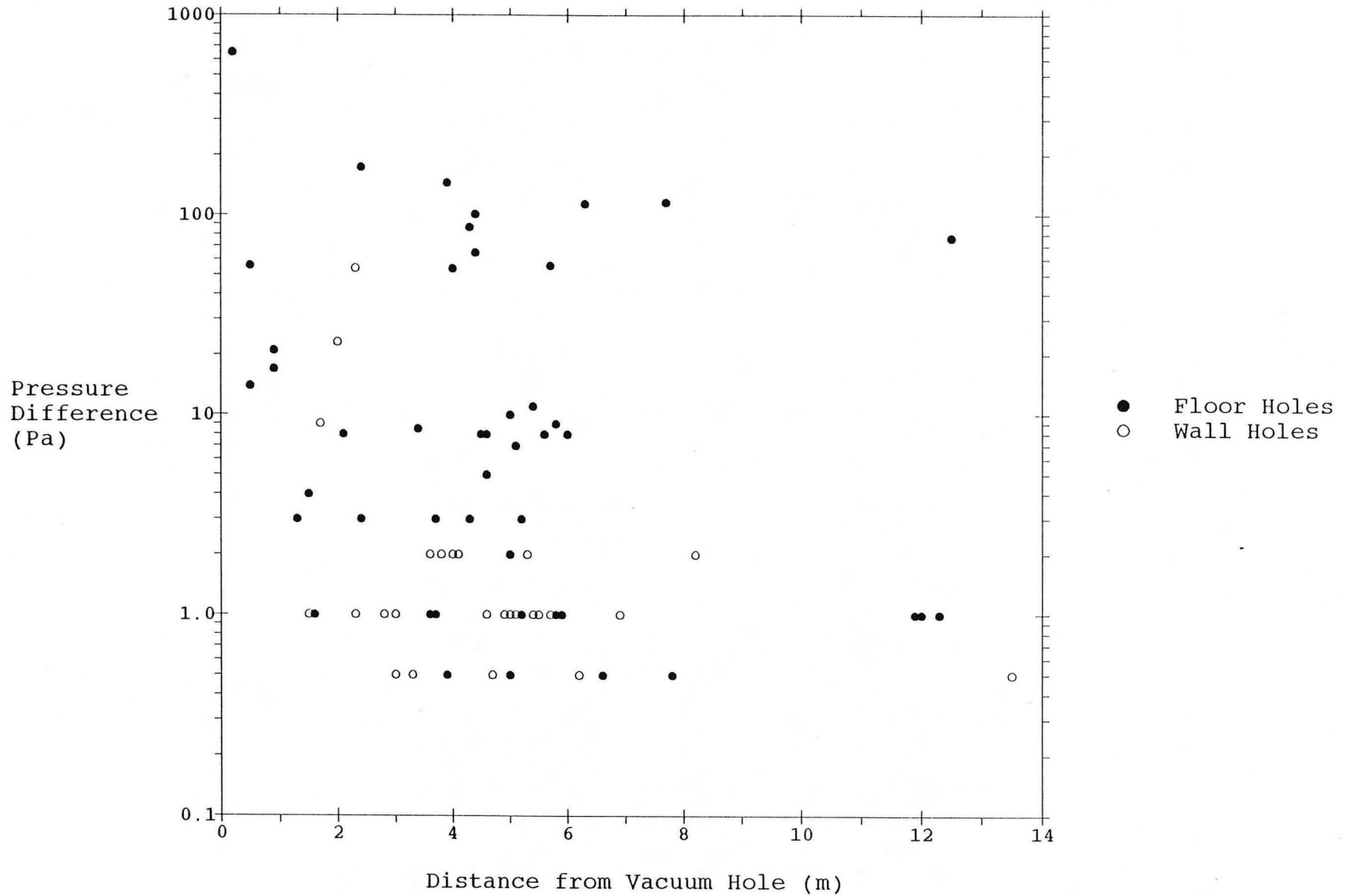
AIR VELOCITIES vs. PRESSURE DIFFERENCES AT TEST HOLES
Both 10 Pa and 30 Pa Basement Depressurization

Air Vel. (m/s)

Pressure (Pa)

● -10 Pa Floor
○ -10 Pa Wall
■ -30 Pa Floor
□ -30 Pa Wall

44
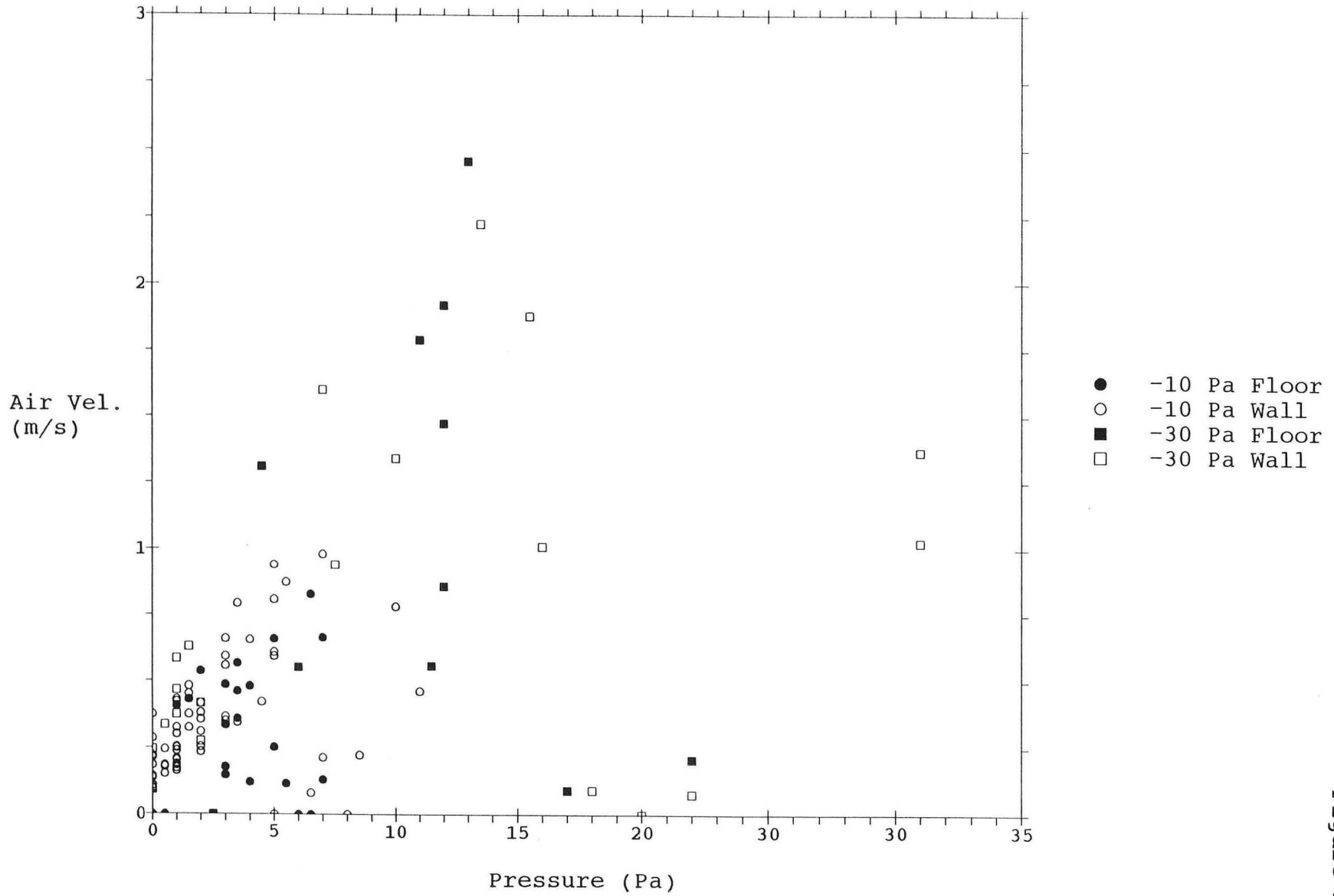
Figure A2

FLOW DETERMINATION AT TEST HOLES:
SMOKE MOVEMENT vs. AIR VELOCITY MEASUREMENTS
Basement Depress. and Vacuum Tests at LBL08, LBL14C

Smoke Flow (relative)
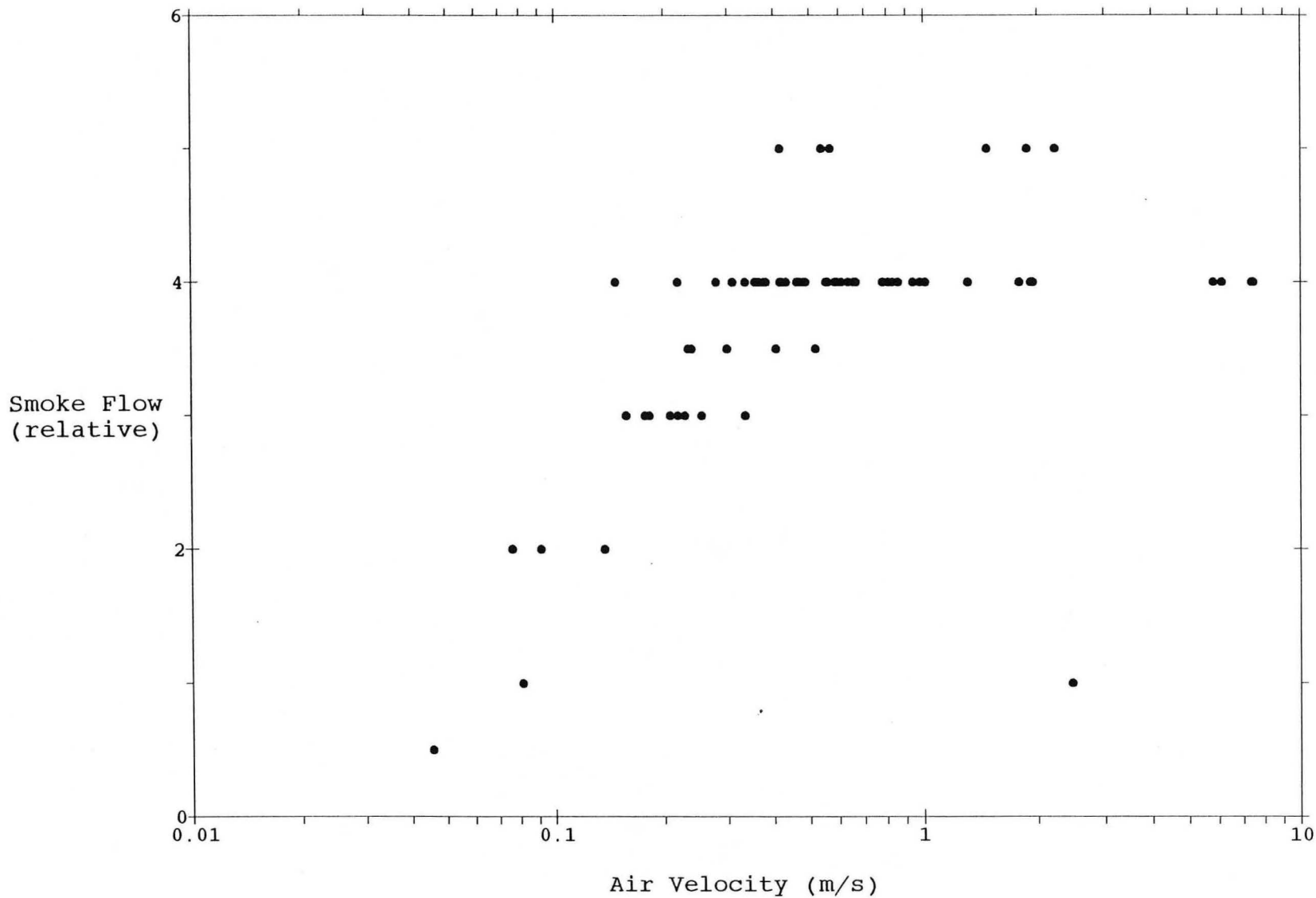
Air Velocity (m/s)

AIR VELOCITY COMPARISONS AT TEST HOLES
Vacuum Test vs. Basement Depress. Test
LBL14C

Depress.
Air Vel.
(m/s)

● −10 Pa Floor
○ −10 Pa Wall
■ −30 Pa Floor
□ −30 Pa Wall

Vacuum− Air Vel. (m/s)
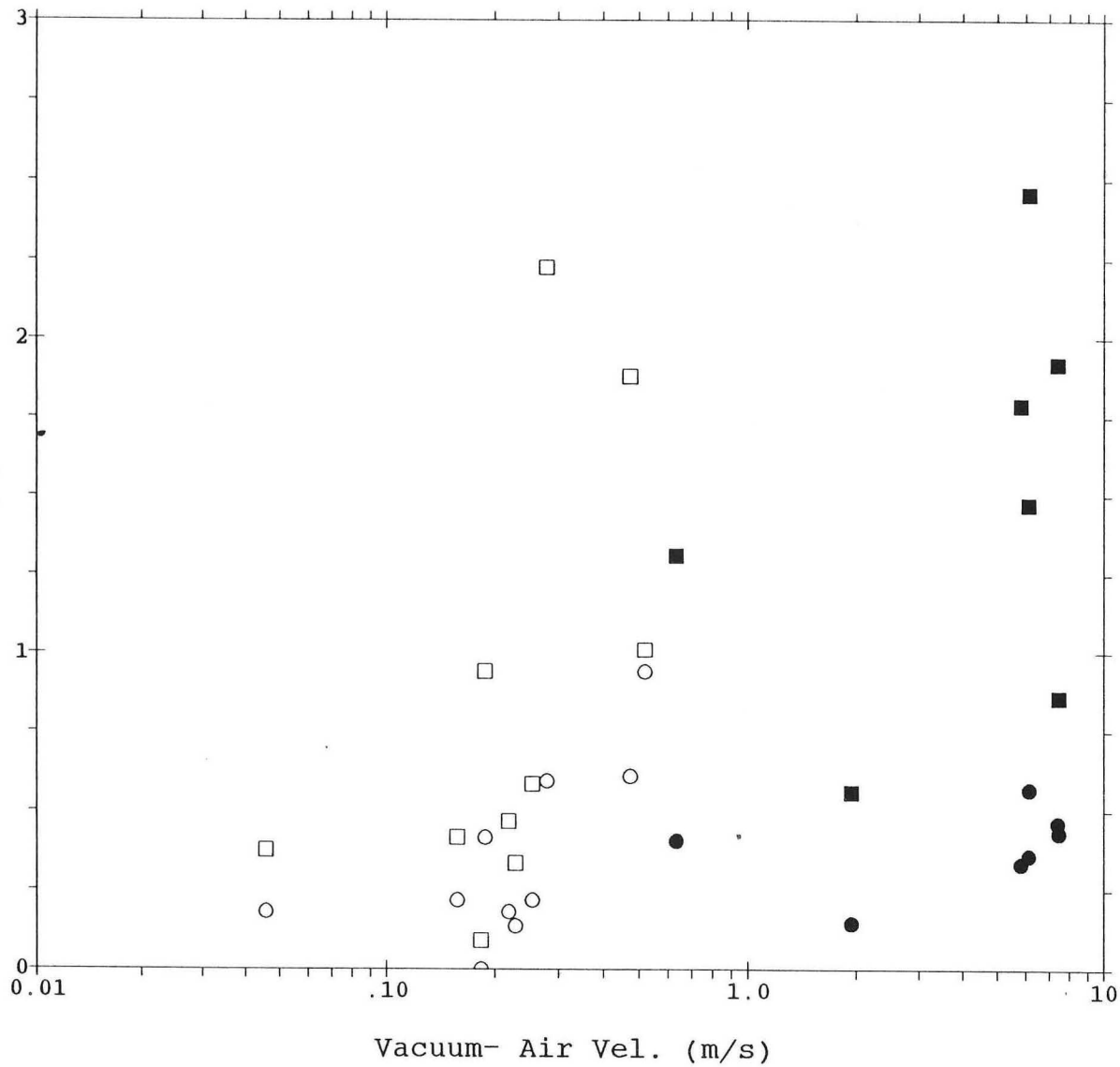
APPENDIX B

Site plans similar to Figure 2 are included for houses LBL08-LBL13 (Figures B1 - B6). Table 1 provides the key to symbols used in these figures. Periodic data that were collected around the time of the diagnostic tests are shown for soil permeability (K) and radon concentrations in grab samples of air (R). Figures B2, B3, and B4 (LBL09, LBL10, LBL11) also contain data for the initial pressure field mapping tests (PFM), that appear in Appendix C for houses LBL08, LBL12, and LBL13. Data from other diagnostic measurements are enclosed in the boxes.

LBL08

Figure B1

48

N ↑

OCN1
K(S)= 420
R(O)= 29

OCN2
K(S)= 460
K(O)= 310
R(N)= 32

OBN1
R(N)= 31

WALKWAY

OAN1
K(S)= 0.3
K(O)= BD
R(O)= 40
R(N)= 49

OAN2
R(N)= 120

OAW3
R(N)= 21

PORCH

IW4(B)
R(D)= 34

FS6
IW6(B)
R(D)= 11

FS7

FS11

OCW1
K(S)= 4
K(O)= 0.09

OBW3
R(N)= 21

SUMP
R(D)= 380

IW5(B)
R(D)= 33

IW7(B)
R(D)= 44

IW8(B)
R(D)= 2.9

IW9(B)
R(D)= 2.7

IW10(B)
R(D)= 5.0

FS5
R(D)= 230

IW3(B)
R(D)= 23

IF8
R(D)= 29

FS9
R(D)= 22

IF9
R(D)= 9.4

OAW2
K(S)= 1500
K(O)= 1500
R(N)= 15

IW2(B)
R(D)= 4.0

IF1
K(S)= 1500
R(D)= 700

IF6
K(S)= 4000
R(O)= 89
R(D)= 150

IF7
K(S)= 0.2
K(O)= 0.3
R(O)= 500
R(D)= 690
R(N)= 380

IW11(B)
R(D)= 1.2

GARAGE

9.6

OBW2
R(N)= 200

IF2
K(S)= 0.5

IF5
K(S)= BD

IW1
K(S)= 4000
K(O)= 2900
R(O)= 20
R(D)= 7.7

IF3
K(S)= BD
K(O)= 0.7
R(O)= 830
R(D)= 120
R(N)= 880

SLAB SEAM
R(D)= 29

OAW1
K(S)= 960
R(O)= 12
R(N)= 11

IW17(B)
R(D)= 1.0

IW18(B)

FS16
R(D)= 13

FS1
R(D)= 290

IW19(B)

IW16(B)
R(D)= 1.4

IW12(B)
R(D)= 1.3

FS20
R(D)= 410

IW23(B)
R(D)= 2.1

IW20(B)
R(D)=23

IF11
R(D)= 19

IF10
R(D)= 0.5

OBW1
R(O)= 24

IW22(B)
R(D)= 3.9

IW21(B)
R(D)= 11

FS13
R(D)= 29

IW13(B)
R(D)= 8.7

OAS4
R(O)= 12

IW15(B)
R(D)= 6.8

IW14(B)

FS12

OAS2
K(S)= 810
R(O)= 75
R(N)= 29

OAS1
K(S)= 260
K(O)= 640
R(O)= 59
R(N)= 46

OAS6
K(S)= 860

OAS3
K(S)= 390
K(O)= 380
R(N)= 14

OBS2
R(N)= 2.0

DECK

OBS1
R(N)= 160

OAS5
K(S)= 10
R(N)= 65

OAS7
K(S)= 270
R(N)= 69

OCS1
K(O)= 23
R(O)= 370
R(N)= 190

Ambient Air Samples (Bq/m³)

Diagnostics (10/31/86)

Basement   6500
Level 1 Liv Rm   1100
Level 1 Spare Rm   1300
Garage   200

Flux Measurements (Bq/m²/s)

10/31/86

Bsmt Flr West   0.0227
S Wall W End   0.0095

Water Samples (Bq/m³)

11/5/86   310,000
8/9/87   140,000

Figure B2

LBL10

N ↑

50

GARAGE

PORCH

BASEMENT

FAMILY RM. SLAB

PATIO

Ambient Air Samples (Bq/m³)

Diagnostics (10/30/86)
Basement 5400
Level 1 Din Rm 2100

Flux Measurements (Bq/m²/s)

10/29/86
Fam Rm Flr NW 0.0137
Bsmt Flr West 0.0120
W Bsmt Wall 1.9307

8/28/87
E Wall Center 0.4730
E Wall S End 0.3023

Water Samples (Bq/m³)

10/31/86 8000
8/4/87 46000

OCN1
PFM=0.90

OCN2
PFM=0.91

OBN1
PFM= 0.81
K(S)= 70
R(S)= 650
R(O1)= 470

OAN1
PFM= 0.72
K(S)= 0.2
K(O1)= 150
R(S)= 60
R(O1)= 26

OAN2
PFM= 0.82
K(S)= 5.4
R(S)= 120
R(O1)= 70

OBW2
PFM= OR

OAW2
K(S)= 0.03
R(S)= 46

OCW2

OBW1
PFM= OR
K(S)= 0.01
R(S)= 110
R(O1)= 4.0

OAW1
PFM= 0.73
K(S)= 70
R(S)= 370
R(O1)= 200

OCW1
PFM= OR

IW13(B)
R(D)= 17

IW12(B)
R(D)= 8.4

IW11(B)

IW10(B)
R(D)= 3.0

IW3
PFM= 0.85
K(S)= 8.4
R(O1)= 13

IF6
R(D)= 340

IW9(B)
R(D)= 4.9

IW14(B)
R(D)= 3.3

IF3
R(D)= 15

IW4
PFM= 0.20
K(S)= 16
K(O1)= 74
R(O1)= 8.6
R(D)= 21

IF2
PFM= 0.43
K(S)= 8.4
R(S)= 110
R(O1)= 28
R(D)= 12

IW8(B)
R(D)= 100

IW15(B)

IF1
PFM= 0.16
K(S)= 13
K(O1)= 27
R(S)= 350
R(O1)= 300
R(D)= 100

IW7
PFM= 0.16
K(S)= 1000
R(S)= 970
R(D)= 190

IW23(B)
R(D)= 75

IW16(B)
R(D)= 5.9

COND. HOLE
R(D)= 41

IW6
PFM= 0.16
K(S)= 4000
R(S)= 670
R(O1)= 420
R(D)= 200

IW17(B)
R(D)= 20

IW5
PFM= 0.89
K(S)= 720
R(S)= 45
R(D)= 16

IF4
R(D)= 20

IW22(B)
R(D)= 28

IF5
R(D)= 57

IW18(B)
R(D)= 5.1

IW19(B)
R(D)= 4.9

IW20(B)

IW21(B)
R(D)= 21

OAS3
PFM= 0.79
K(S)= 5.0
R(S)= 150
R(O1)= 88

OAS2
PFM= 0.74
K(S)= 0.68
R(S)= 150
R(O1)= 64

OAS1
PFM= 0.67
K(S)= 370
K(O1)= 470
R(S)= 210
R(O1)= 190

REGISTER3
R(D)= 3.6

OBS4
K(S)= 0.04

OBS3
K(O1)= BD
K(S)= BD
R(S)= 90

OBS2
PFM= 0.89
K(S)= 0.50
R(S)= 260
R(O1)= 140

OAS4
PFM= 1.0

OCS3
R(O1)= 5.1

OCS2

REGISTER1
R(D)= 2.5

OCE1
PFM= 0.89
R(O1)= 3300

IF7
R(D)= 5.5

OAE1
PFM= 0.88
K(S)= BD
R(S)= 3100
R(O1)= 1900

OCE2
R(O1)= 43

OAE4

OBS1
K(S)= 0.13
R(S)= 6.5

OCS1
K(O1)= BD

5.8

LBL11

N ←

Figure B4

Ambient Air Samples (Bq/m³)

Diagnostics (11/2/86)
Basement	1400
Level 1 Liv Rm	500
Level 2 Hall	400

Flux Measurements (Bq/m²/s)

11/2/86
| Bsmt Flr Center | 0.0048 |
| W Wall S End | 0.1868 |

Water Samples (Bq/m³)

| 11/4/86 | 9000 |
| 8/9/87 | 17000 |

OCE1
PFM= OR
K(O)= BD

OCE2
PFM=1.0
K(O)= 2.6
R(O)= 39

OCE3
R(O)= 52

OBE2
PFM= 0.70
K(O)= 120
R(O)= 32

OBE3
PFM= 0.69
R(O)= 41

OBE4
PFM= 0.71

OBE1
PFM= 1.0
K(O)= BD

OAE1
PFM= 0.68
K(S)= 110
R(S)= 47
R(O)= 20

OAE2
PFM= 0.54
K(S)= 410
K(O)= 720
R(S)= 20
R(O)= 4.0

OAE3
PFM= 0.39
K(O)= 600

7.8

OAN2

OBN1
PFM= OR

GARAGE

OAN1
PFM= OR
K(S)= BD
R(S)= 27
R(O)= 19

IW5(B)

IF5

IW6(B)
R(D)= 1.0

FS3
R(D)= 0.4

IW7(B)
R(D)= 0.1

CRACK3
R(D)= 1.7

IW8(B)
R(D)= 3.6

FS4
R(D)= 3.4

IF6
R(D)= 5.9

IW9(B)
R(D)= 0.8

IW10(B)
R(D)= 3.0

OAS2
PFM= 0.42
R(O)= 7.1

OBS2
PFM= 0.61
K(O)= 1100

OBS3
PFM= 0.55
R(O)= 14

BASEMENT

IF1
PFM= OR
K(S)= BD
R(S)= 0.6
R(D)= 1.4

FS5
R(D)= 12

IW11(B)
R(D)= 9.7

OAS1
PFM= OR
K(S)= 21
K(O)= BD
R(S)= 16
R(O)= 16

CRACK2
R(D)= 1.1

CRACK1
R(D)= 25

IF2
PFM= 0.57
K(S)= 110
R(S)= 17
R(D)= 6.8

IW12(B)
R(D)= 6.7

OBS1
PFM= 0.79
K(O)= 230
R(O)= 37

IF8
R(D)= 7.1

IF7
R(D)= 9.9

IW13(B)
R(D)= 14

OBS4
PFM= 0.93
R(O)= 30

IW4(B)
R(S)= 0.9
R(D)= 0.2

IF4
R(D)= 0.3

IW2(B)
R(D)= 8.2

IW1
PFM= 0R
R(D)=0.6

FS7

IF3
R(D)=0.9

FS1
R(D)=0.8

FS6

OAS3
PFM= OR
R(O)= 19

OCS1
PFM= 1.0

FS2

IW3(B)
R(D)=0.9

IW14(B)
R(D)=7.9

PORCH

OAW1
PFM= 1.0
K(O)= 440
R(O)= 25

OAW2
PFM= 1.0
R(O)= 18

OBW1
PFM= 1.0
K(O)= 7.8
R(O)= 8.7

OBW2
PFM= 1.0
K(O)= 94

OBW3
PFM= 1.0
R(O)= 15

OCW1
PFM= 1.0
K(O)= 1500

LBL12

N ↑

DECK

OAN1
K(S)= 130
K(O)= 130
R(S2)= 180
R(O)= 350

OBN1
K(S)= 880
R(S2)= 830
R(O)= 580

OBN2
K(S)= 16
K(O)= 16
R(S2)= 210

OAN2
K(S)= 300
R(S1)= 400
R(S2)= 800
R(O)= 380

OBN3
K(S)= 3.8
R(S2)= 21
R(O)= 24

OAN3
K(S)= 6.4
R(S1)= 57
R(O)= 44

OCN2
K(O)= 2.8

OBN4
K(S)= 6.5
K(O)= 7.6
R(S2)= 20
R(O)= 33

OAN4
K(S)= 110
K(O)= 2.8
R(S1)= 44
R(S2)= 14

OAN5
K(S)= 46
R(S1)= 44
R(O)= 49

IW19(B)
R(D)= 12

IW20(B)
R(D)= 31
VAC. HOLE

IW21(B)
R(D)= 80

IW7(B)
R(D)= 1.8

IW4
K(S)= 2000
R(S2)= 27
R(D)= 23

IW8(B)
R(D)= 2.0

IW9(B)
R(D)= 2.4

OAE1
K(S)= 130
R(S1)= 69
R(O)= 54

IW18(B)
R(D)= 2.0

CRAWL

IF3
R(D)= 68

IF4
R(D)= 240

OBE1
K(S)= 310
K(O)= 290
R(S1)= 100

CRACK
R(D)= 720

IW2(B)
R(D)= 110

BASEMENT

IW10(B)
R(D)= 9.5

IF7
R(D)= 68

IW22(B)
R(D)= 31

IW3
K(S)= 1500
R(S2)= 860
R(D)= 310

OAE2
K(S)= 520
R(S1)= 93
R(S2)= 140

IW17(B)
R(D)= 21

IW16(B)
R(D)= 1.4

VAC.&
CRM
HOLE

IF2
R(S2)= 300
R(D)= 220

OCE1
R(O)= 95

IF1
R(S2)= 2.5
R(D)= 2.4

IW1
R(D)= 22

IW11(B)
R(D)= 15

OBE2
K(S)= 600
R(S1)= 67
R(S2)= 140
R(O)= 58

IF8
R(D)= 240

IW5
K(S)= 130
R(S2)= 9.2
R(D)= 26

IW15(B)
R(D)= 82

IW6
K(S)= 4000
R(S2)= 130
R(D)= 43

IW13(B)
R(D)= 12

IF5
R(D)= 26

GARAGE

IW14(B)
R(D)= 15

IW12(B)
R(D)= 11

OAE3
K(S)= 300
K(O)= 270.1
R(S1)= 33
R(S2)= 100
R(O)= 42

PORCH

9.7

OAS2
K(S)= 150
R(S1)= 78
R(S2)= 180
R(O)= 170

OAS1
K(S)= 1000
R(S1)= 45
R(O)= 69

OBS1
K(O)= 180

Figure B5

LBL13

N ←

DECK

OCE1 / R(0)= 700
OCE2 / R(0)= 320
OCE3 / R(0)= 110

OBE2 / K(0)= 80 / R(0)= 10
OBE3 / R(0)= 520

OAE1 / R(0)= 76
OAE2 / K(0)= 80 / R(0)= 210
OAE3 / R(0)= 130

OAS1 / K(0)= 1800 / R(0)= 160

OBS1 / K(0)= 19 / R(0)= 140

OAS2 / K(0)= 870 / R(0)= 100

OCS2 / K(0)= 19 / R(0)= 280

OBS2 / K(0)= 620 / R(0)= 230

IW12(B) / R(D)= 8.2
IF4 / R(D)= 200
IW13(B) / R(D)= 13
CRACK1 / R(D)= 580
IW4(B) / R(D)= 6.0
IF5 / R(D)= 550
IW5(B) / R(D)= 6.3

IW1 / K(S)= 2600 / R(S)= 17 / R(0)= 2.5 / R(D)= 1.6
IW2 / K(S)= 2000 / R(S)= 72 / R(0)= 11 / R(D)= 11

CRACK4 / R(D)= 130

OAS3 / K(S)= 250 / K(0)= 240

OAS4 / K(0)= 27 / R(S)= 130

SEWER PIPE / R(D)= 310
IW6(B) / R(D)= 57
IF1 / R(0)= 560 / R(D)= 610

OBS3 / K(S)= 630 / K(0)= 64 / R(S)= 320 / R(0)= 39

OCS1 / K(0)= 4.3 / R(0)= 200

GARAGE

IF6 / R(D)= 68

BASEMENT

IW7(B) / R(D)= 7.6

OIL PIPE / R(D)= 6.8

CRACK5 / R(D)= 60
IW3 / K(S)= 4000 / R(S)= 7.4 / R(0)= 4.8 / R(D)= 7.6
CRACK2 / R(D)= 870
IW8(B) / R(D)= 6.7

IW11(B) / R(D)= 1.6
CRACK3 / R(D)= 94
IF3 / R(D)= 380
IW10(B) / R(D)= 3.6
IW9(B) / R(D)= 12
IF2 / R(D)= 370

OAW2 / K(S)= 650 / K(0)= 660 / R(S)= 43 / R(0)= 24
OAW1 / K(0)= 1200 / R(0)= 13

PORCH

OBW2 / K(0)= 34 / R(0)= 170
OBW1 / K(0)= 170 / R(0)= 13

OCW3 / K(0)= 130 / R(0)= 23
OCW2 / K(0)= 25 / R(0)= 78
OCW1 / K(0)= 23 / R(0)= 230

7.3 m

Ambient air samples (Bq/m³)

Diagnostics (11/4/86)
Basement   4200
Level 1 Fam Rm 2500
Level 2 Hall   2100
Garage   200

Flux Measurements (Bq/m²/s)

11/4/86
S Wall Center   0.0068
Bsmt Flr SW   0.0360

8/27-30/87
S Wall Center Hi   0.0193
S Wall Center Low 0.0126
S Wall Center Hi   0.0104

Water Samples (Bq/m³)

11/5/86   4100
8/4/87   12000

Figure B6

APPENDIX C

Additional sites plans for houses LBL0, LBL12, and LBL13 (Figures C1-C3) that are similar to Figure 3 and included in this appendix. Coupling ratios from pressure field mapping tests (PFM), vacuum field extensions during vacuum tests (V), calculated soil gas entry potentials (G), and calculated radon entry potentials (E) are shown. The location of the final configuration of subsurface depressurization and block wall ventilation pipes is indicated, along with the location of the vacuum test hole.

LBL08

Figure C1

55

N ↑

9.6

WALKWAY

PORCH

GARAGE

DECK

OCN3
PFM(I)= OR

OCN1
PFM(I)= 0.97

OCN2
PFM(I)= 0.87

OBN1
PFM(I)= 0.84

FS6
PFM(10)= 0.40
V= 104

OAN2
PFM(I)= 0.72

OAW3
PFM(I)= 0.90

IW4(B)
PFM(10)=0.20

SSD
PIPE
V= 0
G= 1.4
E= 49

IW6(B)
PFM(10)=0.30
V= 0
G= 1.2
E= 14

FS7
V= 42

IW7(B)
V= 0

IW9(B)
PFM(10)=0.40
V= 0
G= 2.0
E= 5.3

FS11
PFM(10)=0.65
V= 21

IW11(B)
PFM(10)=0.70
V= -21
G= 1.4
E= 1.7

OCW1
PFM(I)= 1.0

OBW3
PFM(I)= 0.87

IW2(B)
PFM(10)=0.10
V= 0
G= 1.1
E= 4.5

IF1
PFM(10)=0.30
V= 150
G= 1.9
E= 1300

IF6
PFM(I)=0.67
PFM(10)=0.30
V= 440
G= 0.6
E= 71

IF8
PFM(10)=0.40
V= 62
G= 1.5
E= 43

IF9
PFM(10)=0.70
V= 21
G= 1.0
E= 9.4

OAW2
PFM)I)= 0.88

VAC. HOLE

IF7
PFM(10)=0.10
V= -21

OBW2
PFM(I)= 0.88

IW1
PFM(I)=0.90
PFM(10)=1.0
V= -42
G= 0.24
E= 3.3

IF3
PFM(I)=0

SSD PIPE

IW16(B)
PFM(10)=0.45
V= 0
G= 1.1
E=1.5

OAW1
PFM(I)= 0.89

IW19(B)
PFM(10)=0.50
V= 0

OBW1
PFM(I)= 0.89

IW20(B)
PFM(10)=0.15
V= 0
G= 2.3
E= 53

IF11
PFM(10)=0.50
V= 21
G= 1.7
E= 33

IW15(B)
PFM(10)=0.20
V= 0
G= 1.6
E= 11

IF10
PFM(10)=0.65
V= 21
G= 1.5
E= 0.8

IW12(B)
PFM(10)=0.20
V= 0
G= 0.9
E= 1.2

IW22(B)
PFM(10)=0.10
V= 0
G= 0.97
E= 3.8

IW23(B)
PFM(10)= 0.10
V= 0
G= 1.5
E= 3.1

OAS4
PFM(I)= 0.89

OAS2
PFM(I)= 0.89

IW14(B)
PFM(10)=0.20
V= 0

FS12
PFM(10)=0.70
V= 0

OAS3
PFM(I)= 0.91

OBS2
PFM(I)= 0.94

OAS5
PFM(I)= 0.91

OAS1
PFM(I)= 0.91

OBS1
PFM(I)= 0.94

OCW2
PFM(I)= OR

OAS7
PFM(I)= 0.96

OCS1
PFM(I)= 0.97

LBL12

N ↑

DECK

OCN1
PFM(I)= 0.77

OCN2
PFM(I)= 0.82

OBN2
PFM(I)= 0.71

OBN3
PFM(I)= OR

OBN4
PFM(I)= 0.85

OBN1
PFM(I)= 0.66

OAN2
PFM(I)= 0.60

OAN3
PFM(I)= OR

OAN4
PFM(I)= 0.81

OAN5
PFM(I)= 0.86

IF4
PFM(10)= 0.55
V= 71
G= 0.24
E= 58

OAN1
PFM(I)= 0.51

BWV
PIPE

IW20(B)
PFM(10)=0.35
V= 0
G= 1.1
E= 130

IF3
PFM(10)=0.50
V= 30
G= 0.60
E= 41

IW7(B)
PFM(10)=0.10
V= 0
G= 0.86
E= 1.5

IW4
PFM(I)=0.85
PFM(10)=0.05
V= 1
G= 0.2
E= 4.3

IW8(B)
V= -0.3

OAE1
PFM(I)= 0.84

IW18(B)
PFM(10)=0.35
V= 0
G= 2.7
E= 24

VAC.
HOLE

IW9(B)
PFM(10)=0.05
V= -0.7
G= 1.0
E= 2.4

IW10(B)
V= 0

IW19(B)
PFM(10)=0.30
V= -0.7
G= 2.0
E= 4.0

CRAWL

IW2(B)
PFM(10)=0.10
V= 0
G= 1.2
E= 130

BASEMENT

OBE1
PFM(I)= 0.84

OBW1
PFM(I)= 0.78

IW22(B)
PFM(10)=0.10
V= 0
G= 1.2
E= 110

IF7
PFM(10)=0
V= 0

IW3
PFM(I)=0.26
PFM(10)=0.70
V= 0.7
G= 0.3
E= 170

IF2
PFM(I)=0.69
PFM(10)=0.05
V= 30
G= 0.05
E= 14

OAE2
PFM(I)= 0.86

OCE1
PFM(I)= 0.31

VAC.&
CRM
HOLE

BWV
PIPE

IW16(B)
V= 0.7

SSD
PIPE

IW17(B)
PFM(10)=0.55
V= 0
G= 2.0
E= 32

IW1
V= 0.3

IF1
PFM(I)=0.65
V= 0

IW11(B)
PFM(10)=0.15
V= 0
G= 2.2
E= 32

IF6
PFM(10)=0.40
V= 45
G= 0.34
E= 81

IW5
PFM(I)=0.86
PFM(10)=0.80
V= 0.3
G= 0.01
E= 0.2

OBE2
PFM(I)= 0.82

IW15(B)
PFM(10)=0.10
V= 0.7
G= 2.3
E= 190

GARAGE

IW12(B)
PFM(10)=0.15
V= 0
G= 1.4
E= 16

OAE3
PFM(I)= 0.78

IW6
PFM(I)=0.77
V= 0.7

IW14(B)
PFM(10)=0.10
V= 0
G= 1.7
E= 25

IF5
PFM(10)=0.65
V= 30
G= 0.02
E= 0.5

PORCH

OAS2
PFM(I)= 0.83

OAS1
PFM(I)= 0.84

OBS2
PFM(I)= 0.85

OBS1
PFM(I)= 0.84

Figure C2

LBL13

N ←

DECK

$\overline{OCE1}$
PFM(I)= 1.0

$\overline{OCE2}$
PFM(I)= 0.91

$\overline{OCE3}$
PFM(I)= 0.90

$\overline{OBE1}$
PFM(I)= 1.0

$\overline{OBE3}$
PFM(I)= 0.85

IF5
PFM(10)= 0
PFM(30)= 0.7
V= 0
G= 0.03
E= 14

IW5(B)
PFM(10)= 0
PFM(10)= 0.04
PFM(30)= 0
V= -0.4
G= 0.25
E= 1.6

$\overline{OAE1}$
PFM(I)= 0.89

$\overline{OAE2}$
PFM(I)= 0.94

$\overline{OAE3}$
PFM(I)= 0.77

$\overline{OAS1}$
PFM(I)= 0.79

$\overline{OBS1}$
PFM(I)= 0.35

IF4
PFM(10)= 0.43
PFM(30)= 0.46
V= 0
G= 0.04
E= 8.2

IW12(B)
PFM(10)=0.30
PFM(10)=0.21
PFM(30)=0.27
V= -0.4
G= 1.4
E= 11

IW1
PFM(I)=0.80
PFM(10)=0.79
PFM(30)=0.84
V=0.8
G=0.32
E=2.2

IW4(B)
PFM(10)=0.10
PFM(10)=0
V= -0.4
G= 1.1
E= 6.7

$\overline{OAS2}$
PFM(I)= 0.73

$\overline{OCS2}$
PFM(I)= 0.82

IW13(B)
PFM(10)=0.10
PFM(10)=0.11
V= 0
G= 1.1
E= 14

IW2
PFM(I)=0.73
V= 4

$\overline{OBS2}$
PFM(I)= 0.71

GARAGE

IF1
PFM(I)=0.39
V= 277

VAC.
HOLE

$\overline{OAS3}$
PFM(I)= 0.75

$\overline{OBS3}$
PFM(I)= 0.71

IW6(B)
PFM(10)=0
PFM(10)=0
PFM(30)=0
V= -0.4
G= 0.24
E= 13

IF6
V= 0

BASEMENT

$\overline{OAS4}$
PFM(I)= 0.73

SSD
PIPE

IW7(B)
PFM(10)= 0
PFM(10)= 0
PFM(30)= 0
V= -0.4
G= 0.60
E= 4.6

IW3
PFM(I)=0.03
PFM(10)=0.07
PFM(30)=0.05
V= -0.4
G= 0.9
E= 6.0

IW8(B)
PFM(10)= 0
PFM(10)= 0.04
V= -0.4
G= 0.81
E= 5.4

IW11(B)
PFM(10)=0.20
PFM(10)=0.21
PFM(30)=0.19
V= 0
G= 1.7
E= 2.6

IW10(B)
PFM(10)=0.10
PFM(10)=0.07
V= -0.4
G= 1.3
E= 3.3

IW9(B)
PFM(10)=0.10
PFM(10)=0
PFM(30)=0.04
V= -0.4
G= 1.3
E= 16

IF2
PFM(10)= 0.50
PFM(30)= 0.59
V= 1
G= 0.16
E= 59

IF3
V= 0.2

$\overline{OAW2}$
PFM(I)= 0.60

$\overline{OAW1}$
PFM(I)= 0.69

PORCH

$\overline{OBW2}$
PFM(I)= 0.67

$\overline{OBW1}$
PFM(I)= 0.73

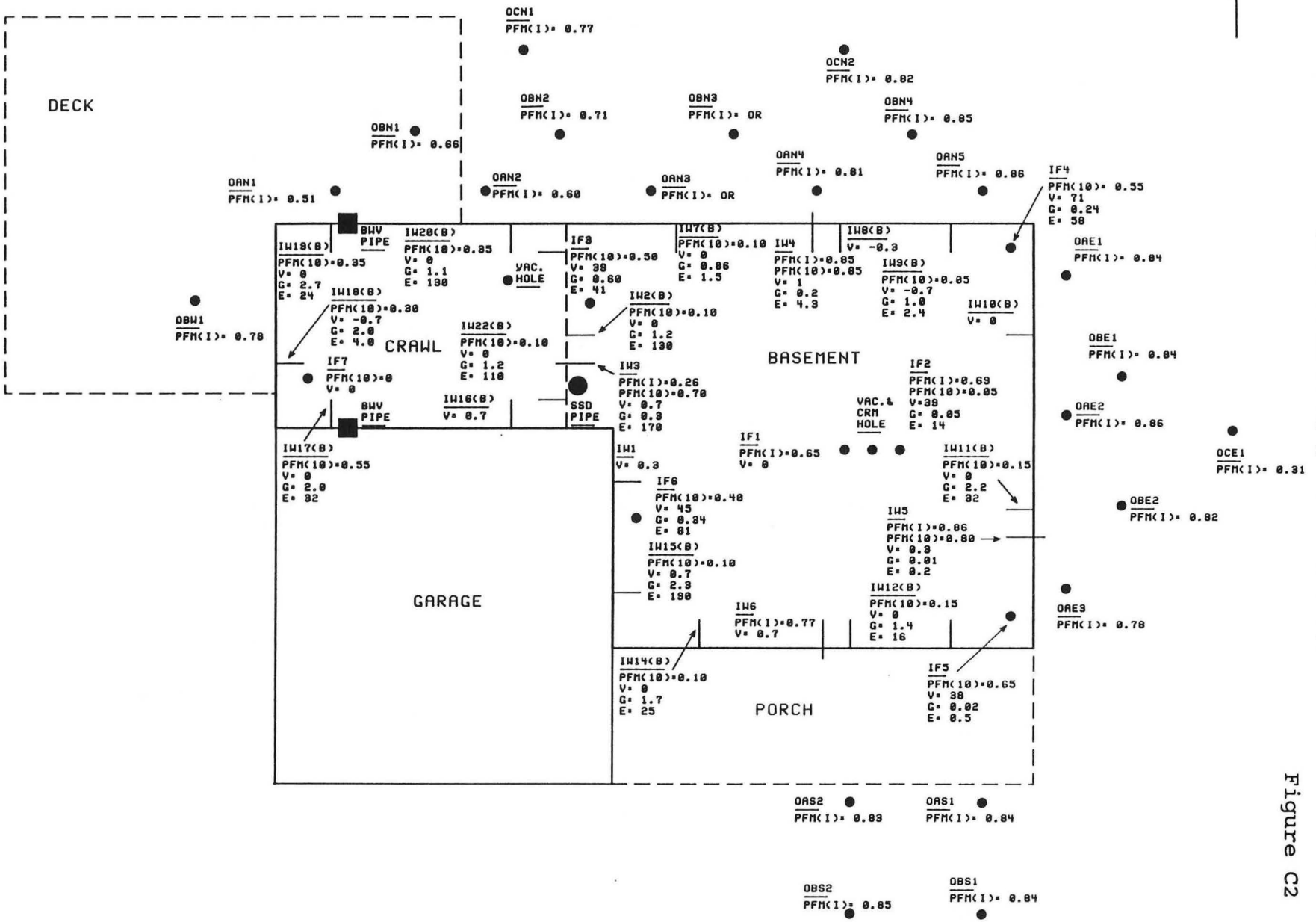$\overline{OCW3}$
PFM(I)= 0.77

$\overline{OCW2}$
PFM(I)= 0.79

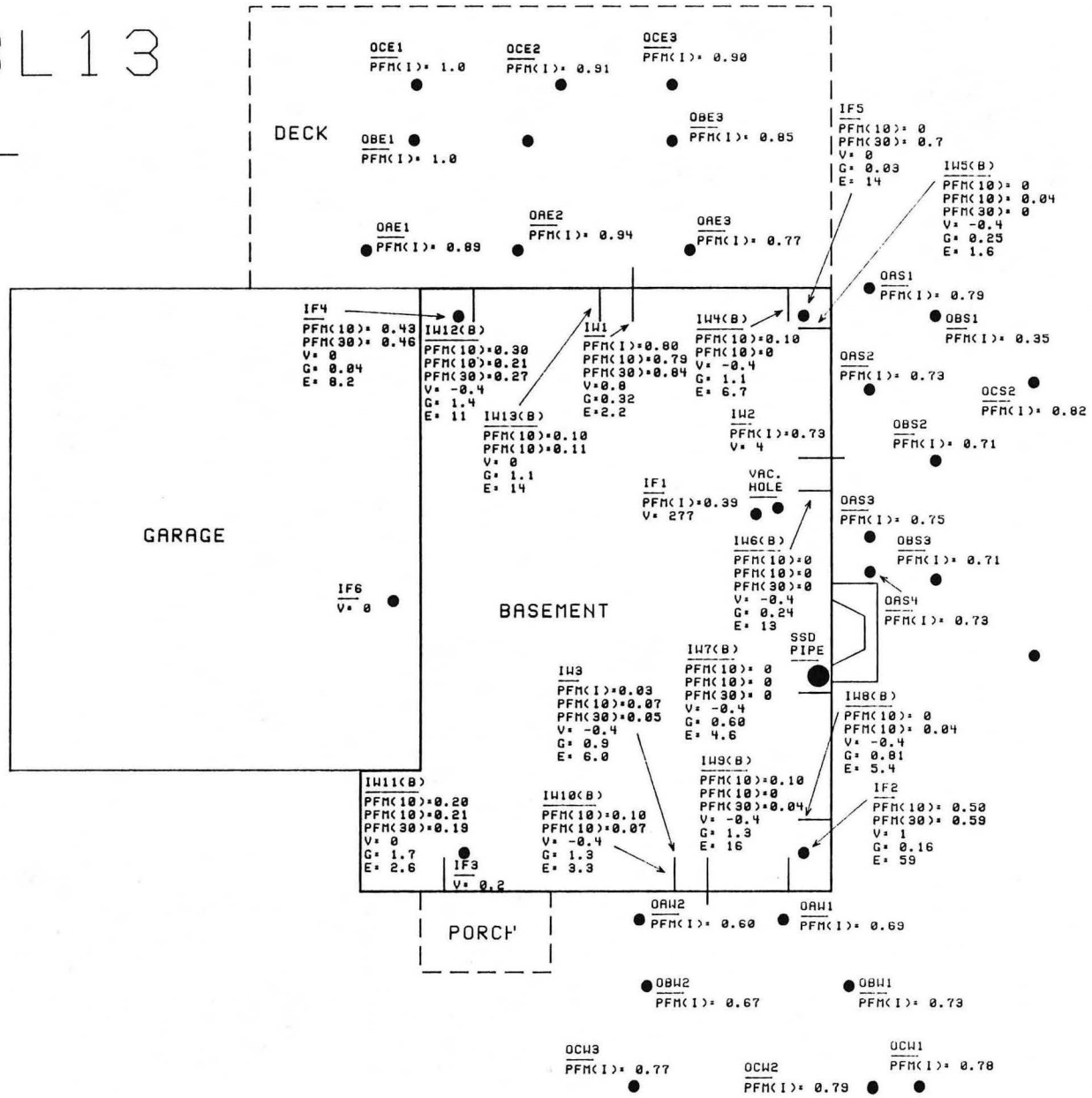$\overline{OCW1}$
PFM(I)= 0.78

7.3

Figure C3

LAWRENCE BERKELEY LABORATORY
TECHNICAL INFORMATION DEPARTMENT
1 CYCLOTRON ROAD
BERKELEY, CALIFORNIA 94720